Supporting Information

Photothermal activation of metal-organic frameworks using a UV-Vis light source

Jordi Espín,[†] Luis Garzón-Tovar, [†] Arnau Carné-Sánchez, [†] Inhar Imaz[*†] and Daniel Maspoch[*†‡]

[†]Catalan Institute of Nanoscience and Nanotechnology (ICN2), CSIC and The Barcelona Institute of Science and Technology, Campus UAB, Bellaterra, 08193 Barcelona, Spain.

[‡]ICREA, Pg. Lluís Companys 23, 08010 Barcelona, Spain.

E-mail: inhar.imaz@icn2.cat, daniel.maspoch@icn2.cat

Section S1. UV-Vis lamp irradiance calibration

Figure S1. Plot of UV-Vis irradiance of the lamp as a function of the inverse squared light guide to sample distance.

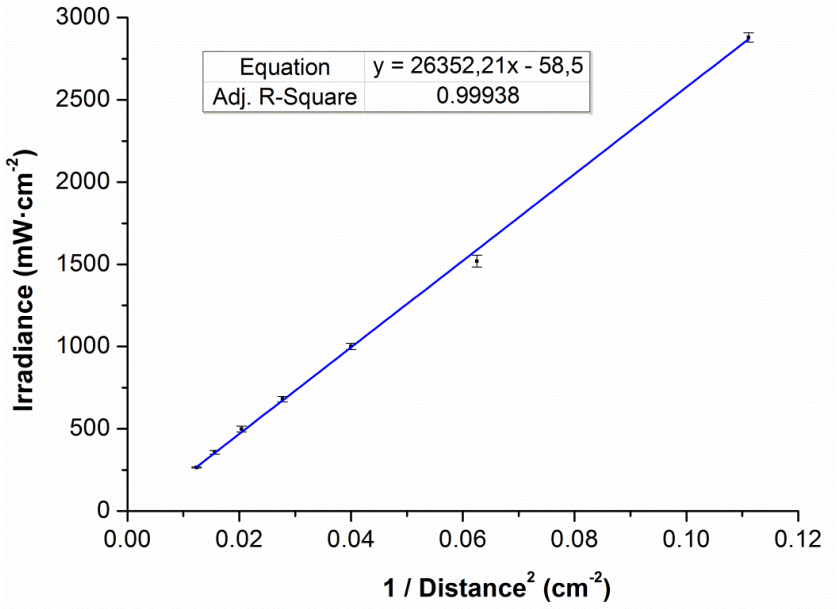

Section S2. Activation setup description

Figure S2. Picture showing the activation setup. In it, the sample is placed in a three-neck round bottom flask and the light guide set at the desired distance from the powder. Ar flow is applied using an inlet needle through a septum, and it is then purged through an outlet one. The light guide neck is capped using parafilm. Once the whole setup is covered to avoid UV light damage, the sample is irradiated for a certain period of time.

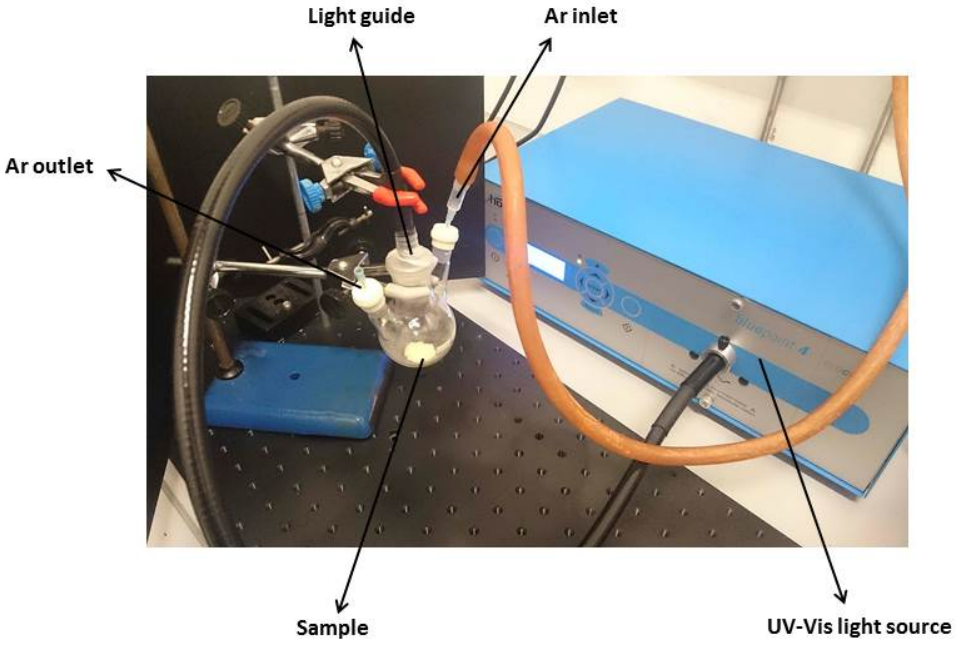

Section S3. HKUST-1 characterization

Figure S3. (Top) Photographs of HKUST-1 powder before and after UV-Vis irradiation (500 mW·cm^{-2} for 30 min). (Bottom) Infrared camera images of HKUST-1 before and during UV-Vis irradiation.

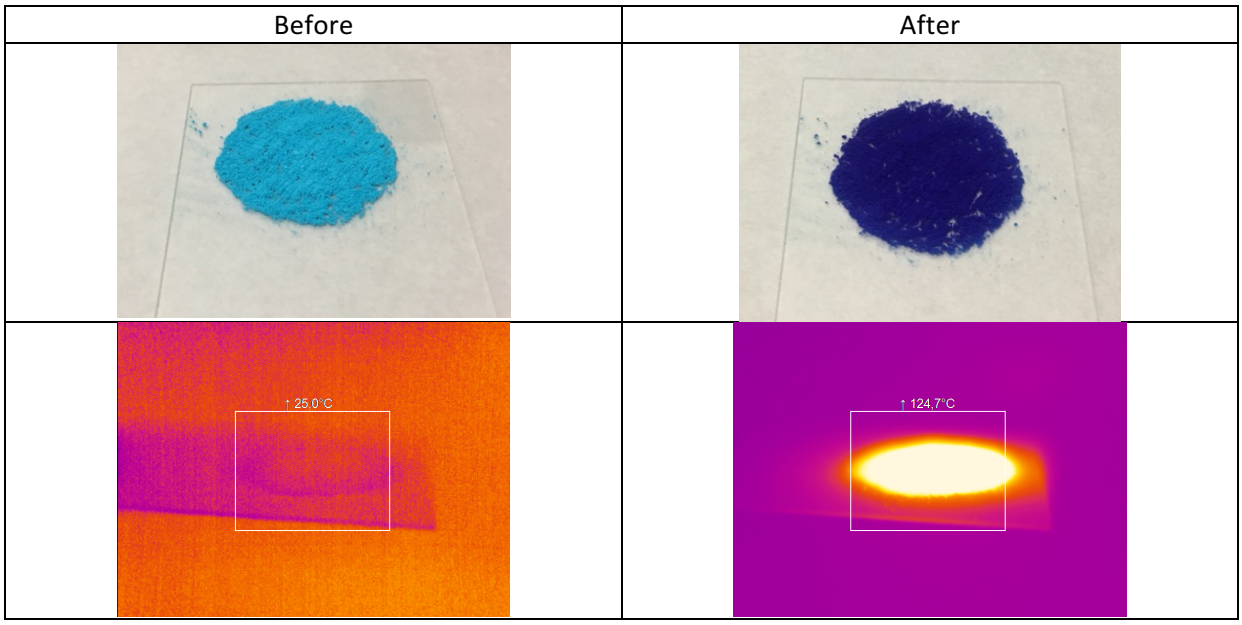

Figure S4. Solid-state UV-Vis spectra of HKUST-1 (red) and 1,3,5-benzenetricarboxylic acid (BTC) (black).

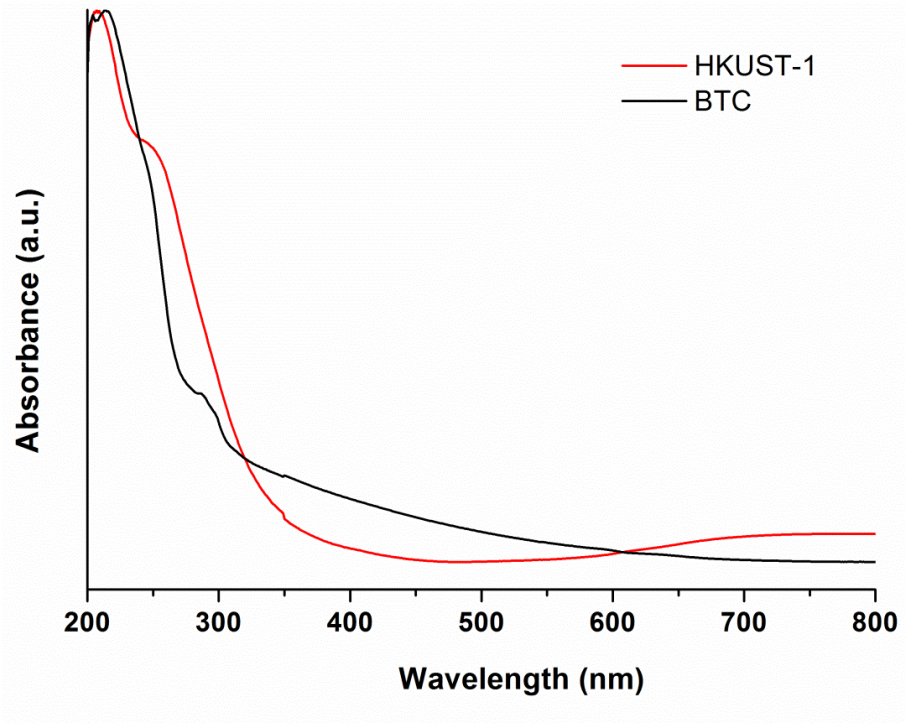

Figure S5. Solid-state UV-Vis spectra of HKUST-1 (red) and BTC (black) in the range of 600-800 nm.

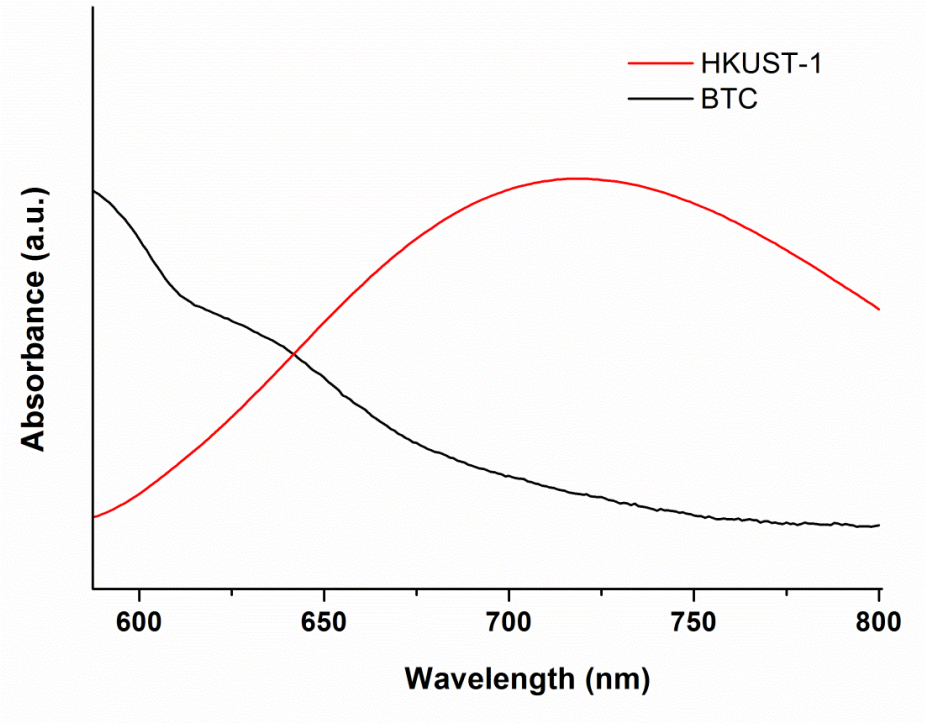

Figure S6. a) Solid-state UV-Vis spectra of HKUST-1 highlighting the wavelength range (green: 300-650 nm; blue: 320-390 nm; red: 390-500 nm). b) Temperature evolution as a function of time for HKUST-1 irradiated at a distance of 7 cm and in a wavelength range of 320-390 nm (blue), 390-500 nm (red) and 300-650 nm (green).

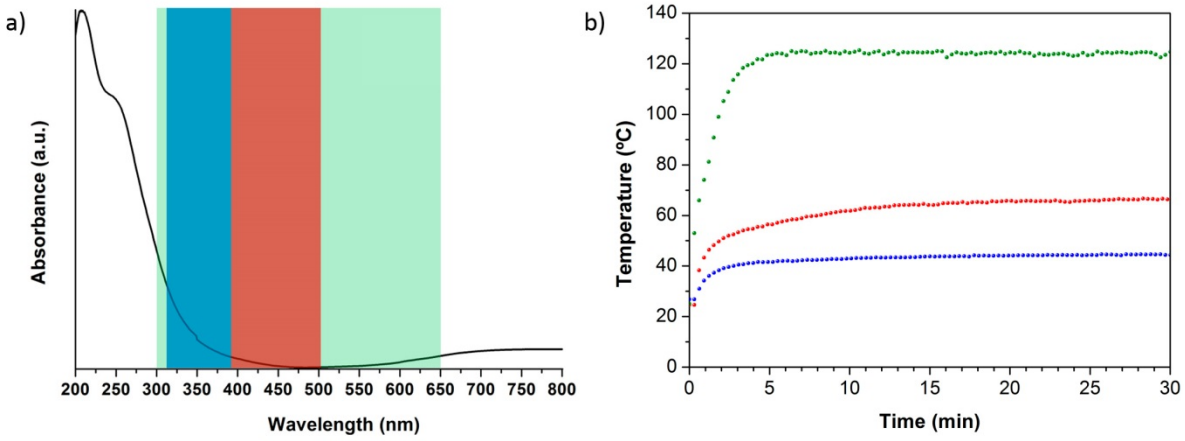

Figure S7. X-Ray Powder Diffraction (XRPD) patterns of HKUST-1 simulated (black), as made (red) and after UV-Vis irradiation at 500 mW·cm^{-2} for 5 min (blue) and 30 min (green).

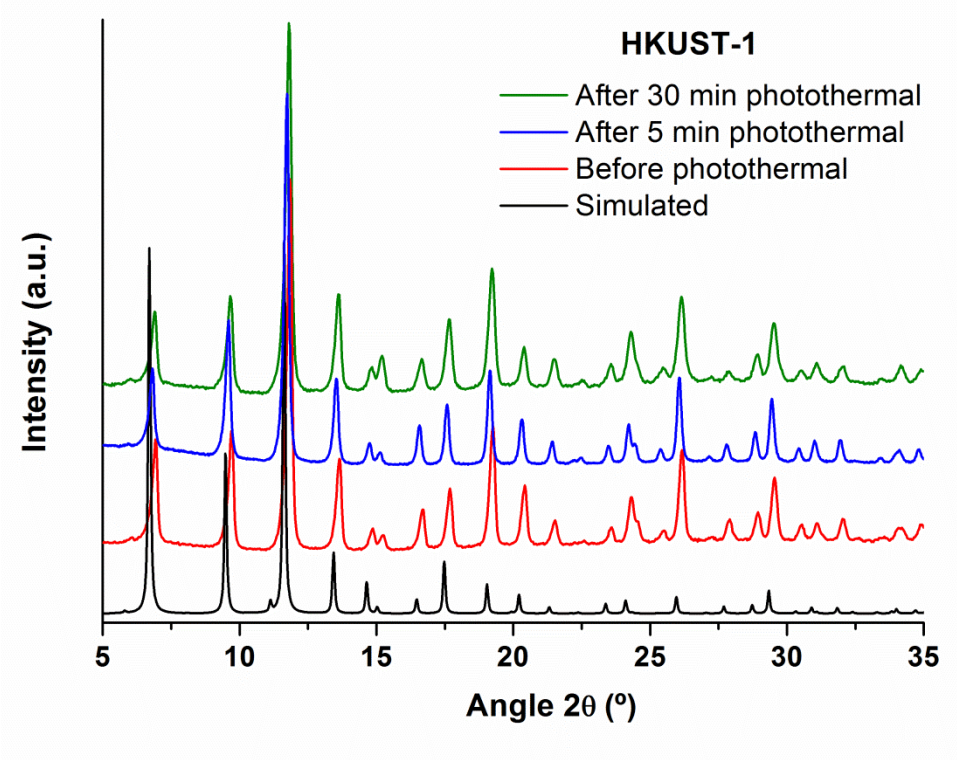

Figure S8. N_2 adsorption isotherm and linear fit of the pressure range used to calculate BET area for HKUST-1 after UV-Vis irradiation at 500 mW·cm^{-2} for 5 min.

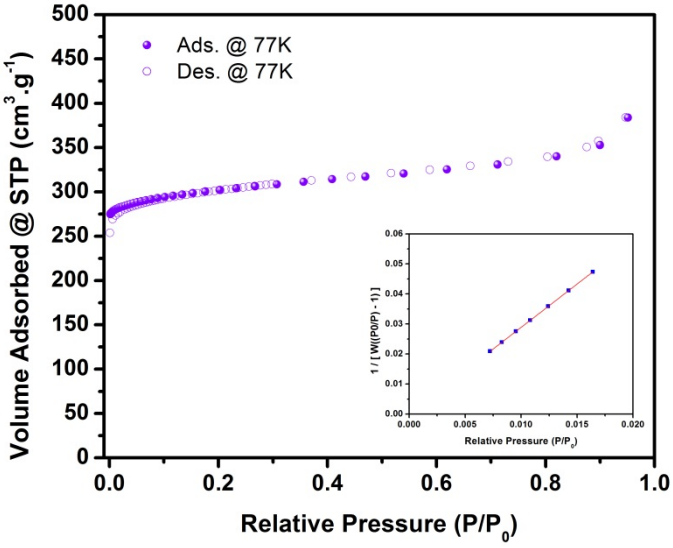

BET surface area: 1208.524 m²·g^{-1}

Slope: 2.882 g·cm^{-3} STP

Intercept: 7.720e-05 g·cm^{-3} STP

Correlation coefficient: 1.00000

C constant: 37324.475

Molecular cross-sectional area: 0.1620 nm²

Figure S9. N_2 adsorption isotherm and linear fit of the pressure range used to calculate BET area for HKUST-1 after UV-Vis irradiation at 500 mW·cm^{-2} for 30 min.

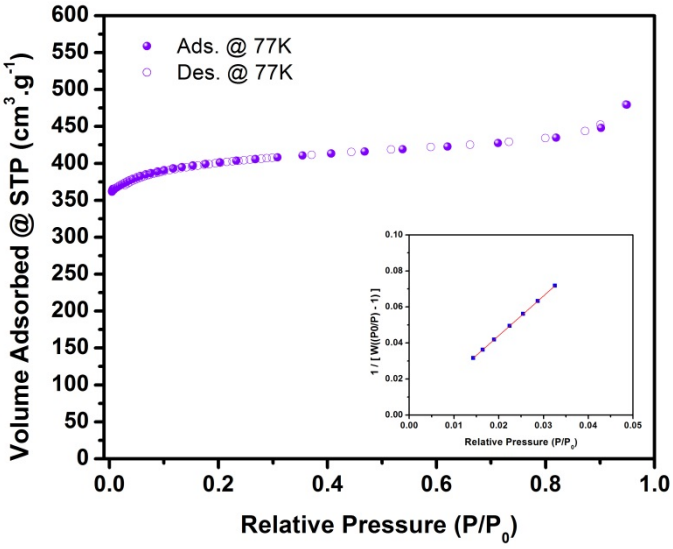

BET surface area: 1583.474 m²·g^{-1}

Slope: 2.199 g·cm^{-3} STP

Intercept: 1.063e-04 g·cm^{-3} STP

Correlation coefficient: 1.00000

C constant: 20692.377

Molecular cross-sectional area: 0.1620 nm²

Figure S10. N_2 adsorption isotherm and linear fit of the pressure range used to calculate BET area for HKUST-1 after heat treatment for 30 min.

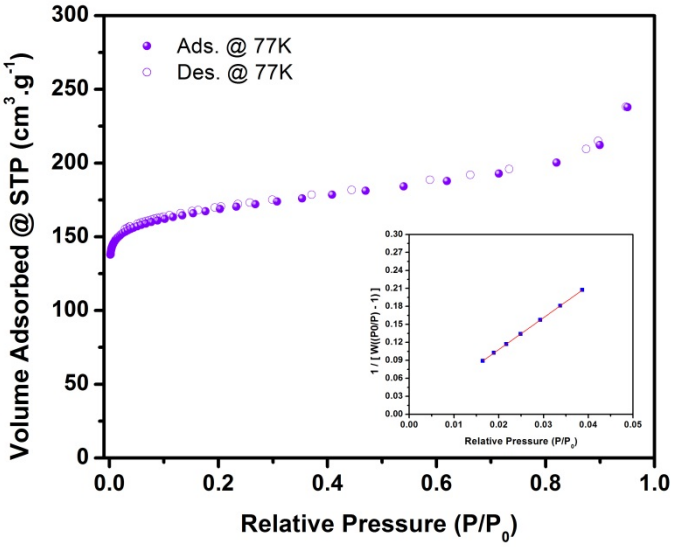

BET surface area: 655.551 m²·g^{-1}

Slope: 5.311 g·cm^{-3} STP

Intercept: 1.832e-03 g·cm^{-3} STP

Correlation coefficient: 0.999998

C constant: 2899.543

Molecular cross-sectional area: 0.1620 nm²

Figure S11. Temperature evolution as a function of time for HKUST-1 irradiated at 900 mW·cm^{-2} (distance = 5 cm) for 30 min.

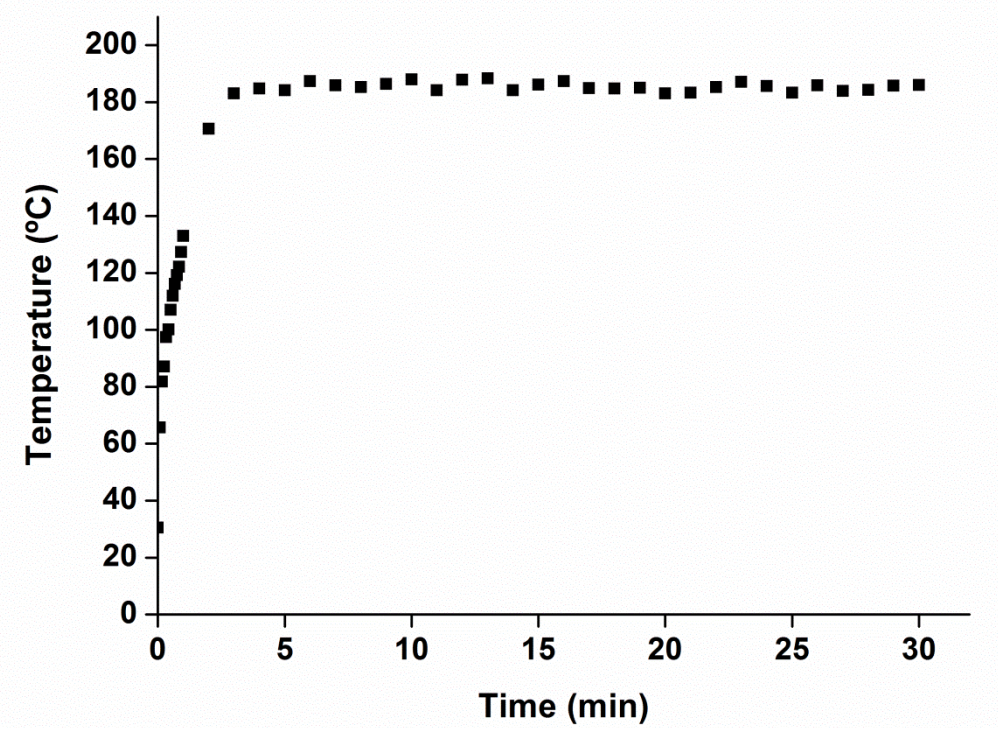

Figure S12. XRPD patterns of as made HKUST-1 (black), and after UV-Vis irradiation for 5 min at 900 mW·cm^{-2} (red) and at 2650 mW·cm^{-2} (blue).

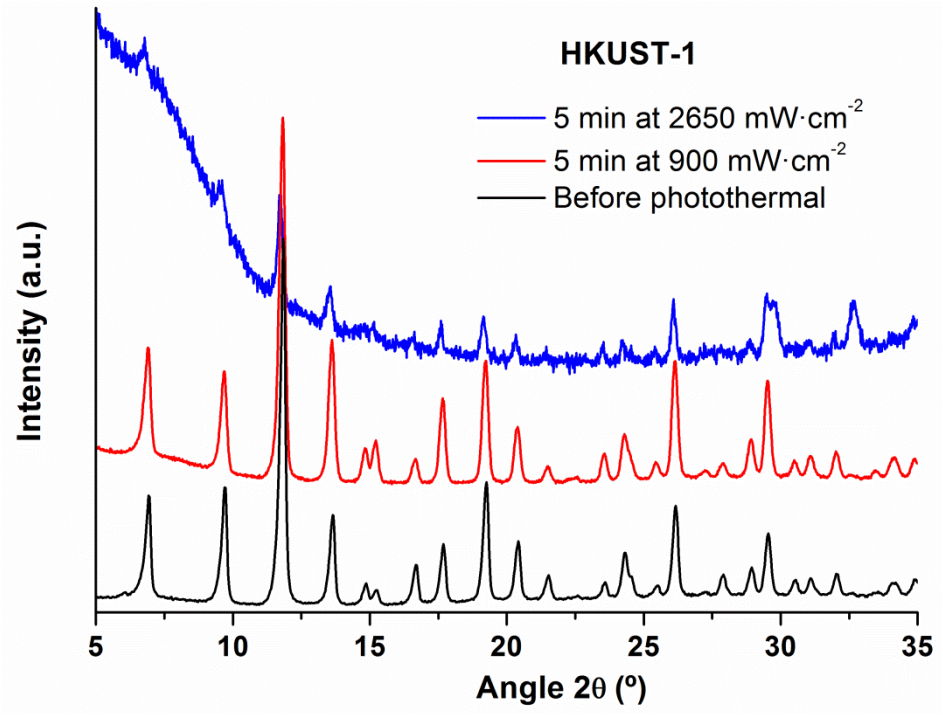

Figure S13. N_2 adsorption isotherm and linear fit of the pressure range used to calculate BET area for HKUST-1 after UV-Vis irradiation at 900 mW·cm^{-2} for 30 min.

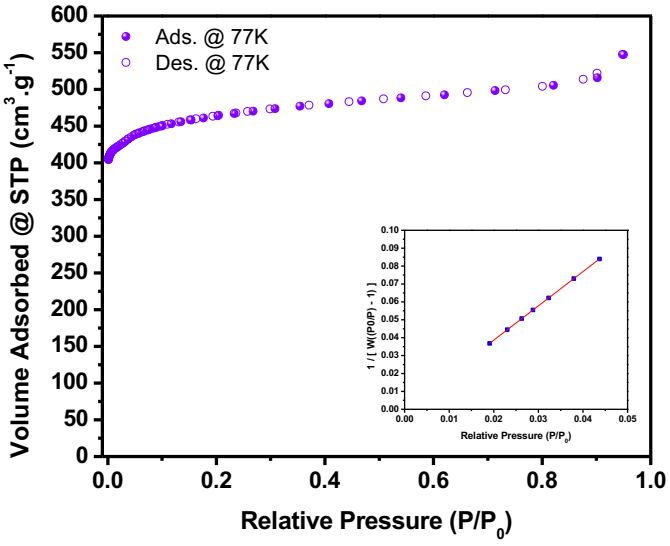

BET surface area: 1819.128 m²/g

Slope: 1.914 g/cm^3 STP

Intercept: 3.788e-04 g/cm^3 STP

Correlation coefficient: 0.999997

C constant: 5053.383

Molecular cross-sectional area: 0.1620 nm²

Figure S14. ^{1}H NMR spectrum of the photothermally activated HKUST-1 once digested in DCl/DMSO-d_6.

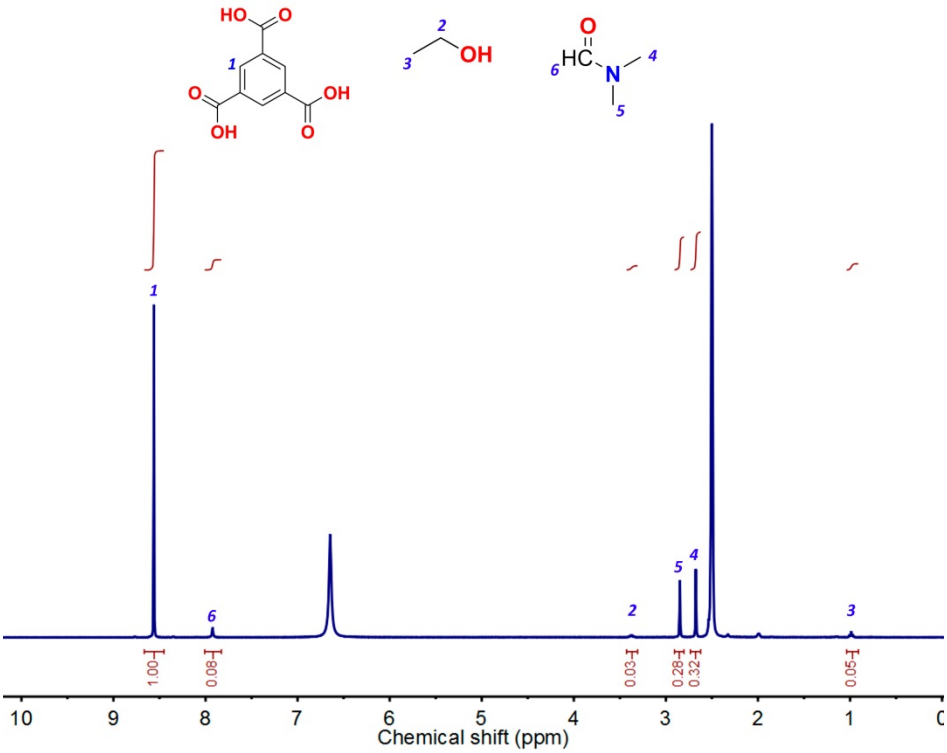

Section S4. UiO-66-X characterization

Figure S15. (Top) Photographs of UiO-66 powder before and after UV-Vis irradiation (500 mW·cm^{-2} for 30 min). (Bottom) Infrared camera images of UiO-66 before and during UV-Vis irradiation.

Before	After
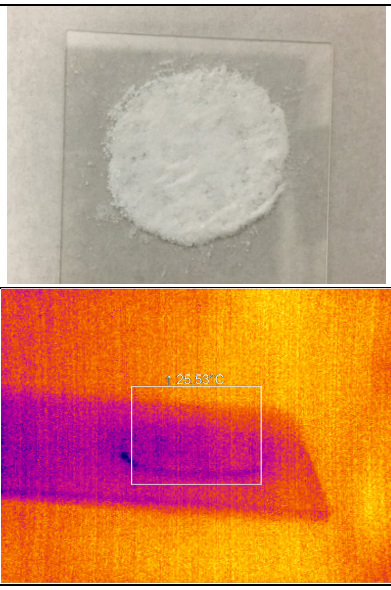	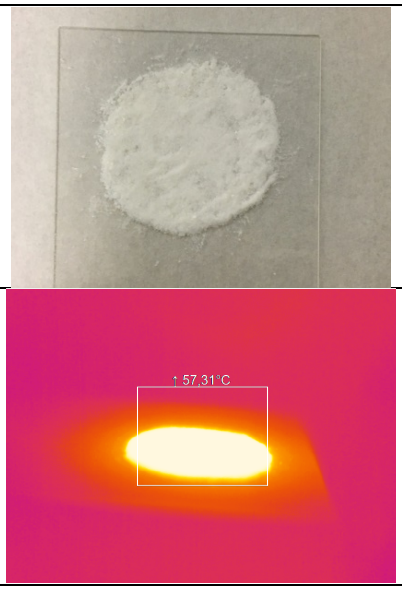

Figure S16. (Top) Photographs of UiO-66-NH_2 powder before and after UV-Vis irradiation (500 mW·cm^{-2} for 30 min). (Bottom) Infrared camera images of UiO-66-NH_2 before and during UV-Vis irradiation.

Before	After
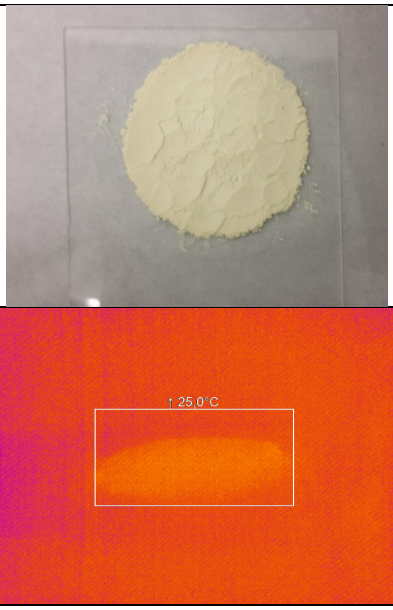	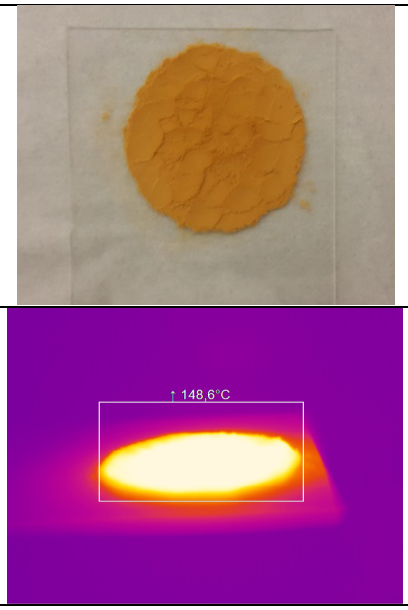

Figure S17. Solid-state UV-Vis spectra of UiO-66 (red) and 1,4-benzenedicarboxylic acid (BDC) (black).

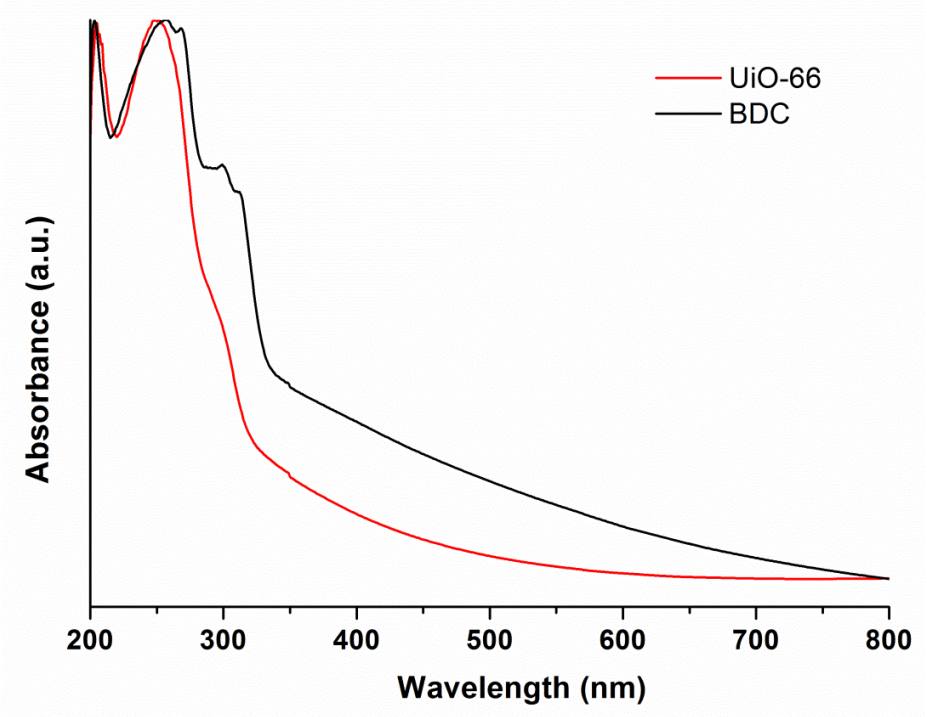

Figure S18. Solid-state UV-Vis spectra of UiO-66-NH_2 (red) and 2-aminoterephtalic acid (BDC- NH_2) (black).

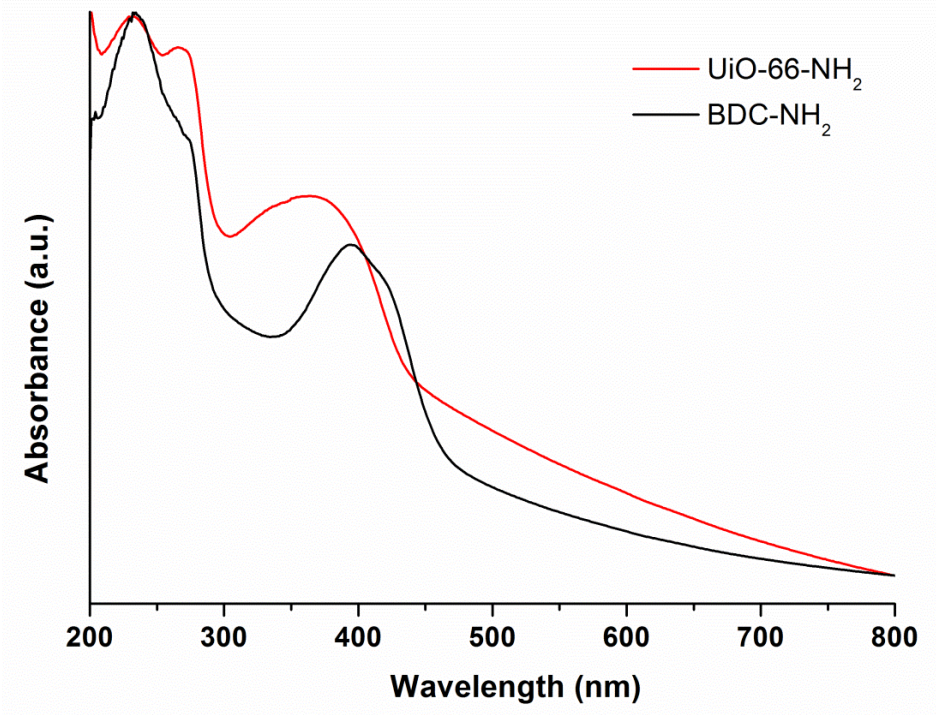

Figure S19. XRPD patterns of UiO-66 simulated (black), as made (red) and after UV-Vis irradiation at 500 mW·cm^{-2} for 30 min (blue).

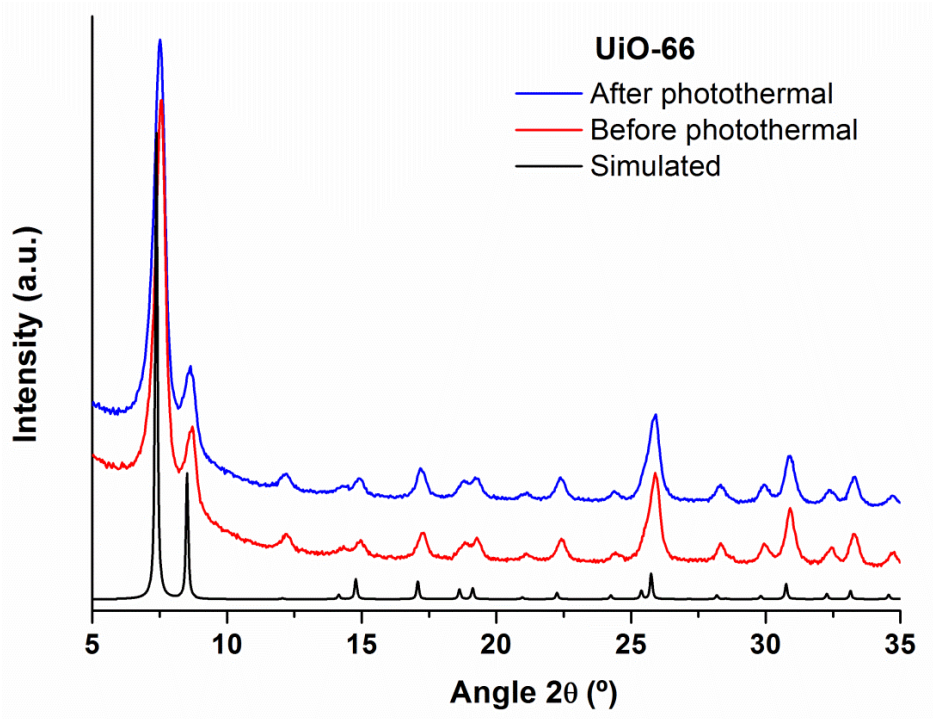

Figure S20. XRPD patterns of UiO-66-NH_2 simulated (black), as made (red) and after UV-Vis irradiation at 500 mW·cm^{-2} for 30 min (blue).

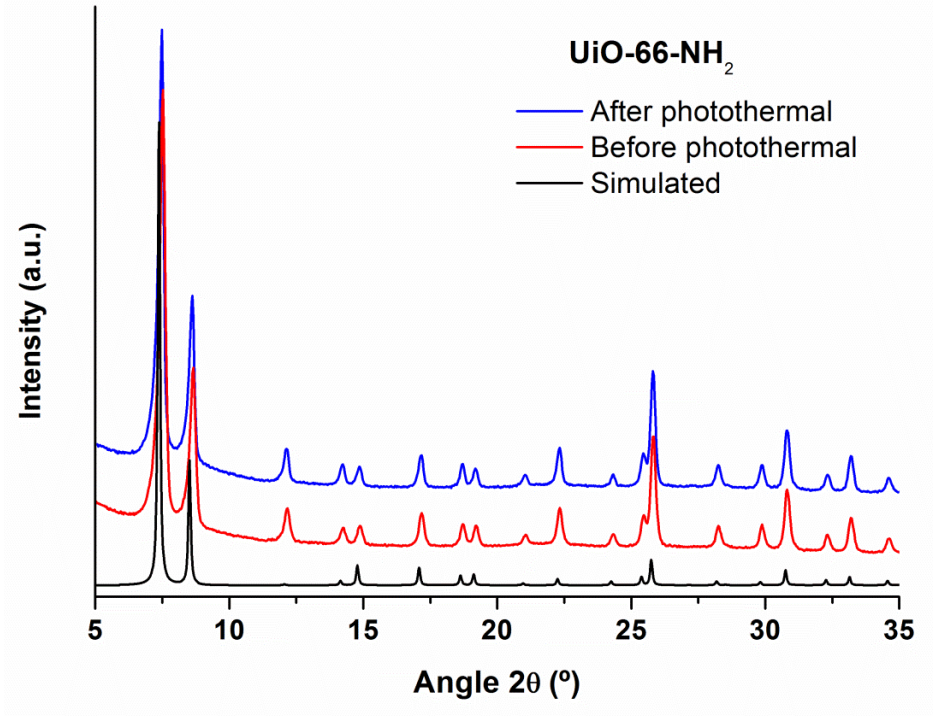

Figure S21. N_2 adsorption isotherm and linear fit of the pressure range used to calculate BET area for UiO-66 after UV-Vis irradiation at 500 mW·cm^{-2} for 30 min.

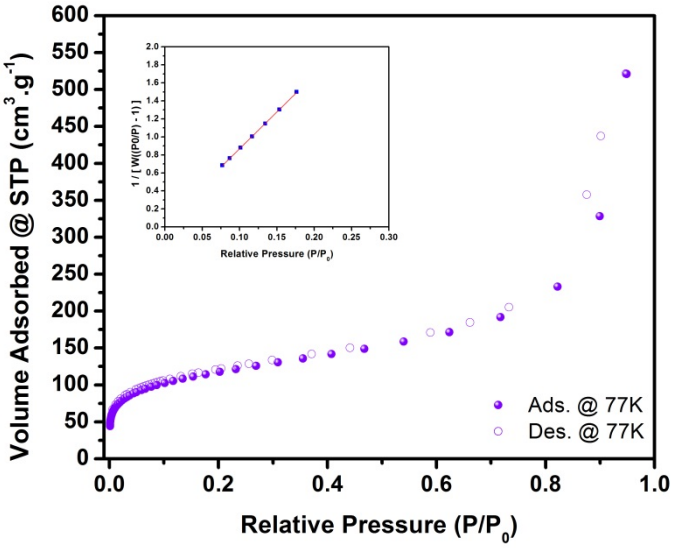

BET surface area: 423.635 m²·g^{-1}

Slope: 8.168 g·cm^{-3} STP

Intercept: 5.226e-02 g·cm^{-3} STP

Correlation coefficient: 0.999938

C constant: 157.290

Molecular cross-sectional area: 0.1620 nm²

Figure S22. N_2 adsorption isotherm and linear fit of the pressure range used to calculate BET area for UiO-66-NH_2 after UV-Vis irradiation at 500 mW·cm^{-2} for 30 min.

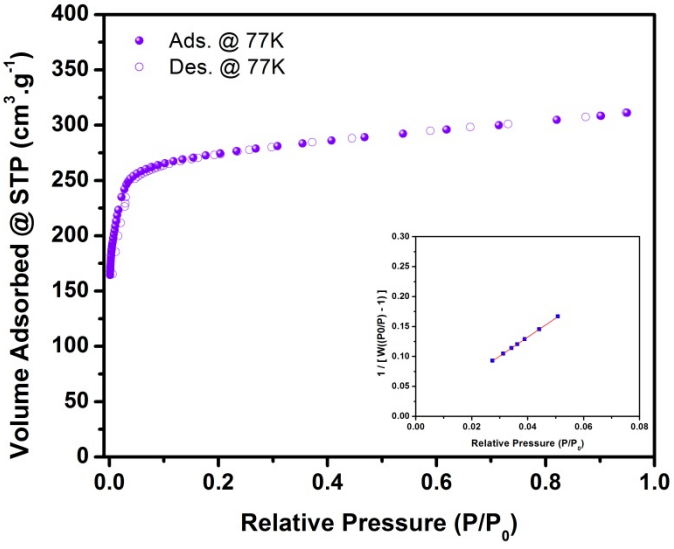

BET surface area: 1098.267 m²·g^{-1}

Slope: 3.165 g·cm^{-3} STP

Intercept: 5.832e-03 g·cm^{-3} STP

Correlation coefficient: 0.999913

C constant: 543.733

Molecular cross-sectional area: 0.1620 nm²

Figure S23. ^{1}H NMR spectrum of the photothermally activated UiO-66 once digested in HF/DMSO-d_6.

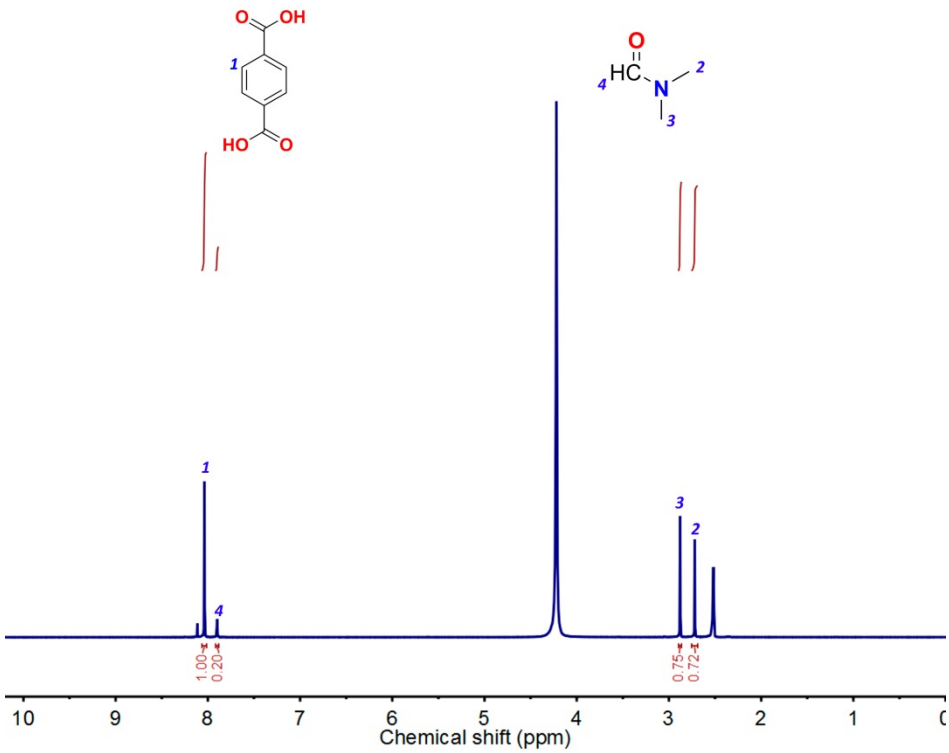

Figure S24. ^{1}H NMR spectrum of the photothermally activated UiO-66-NH_2 once digested in HF/DMSO-d_6.

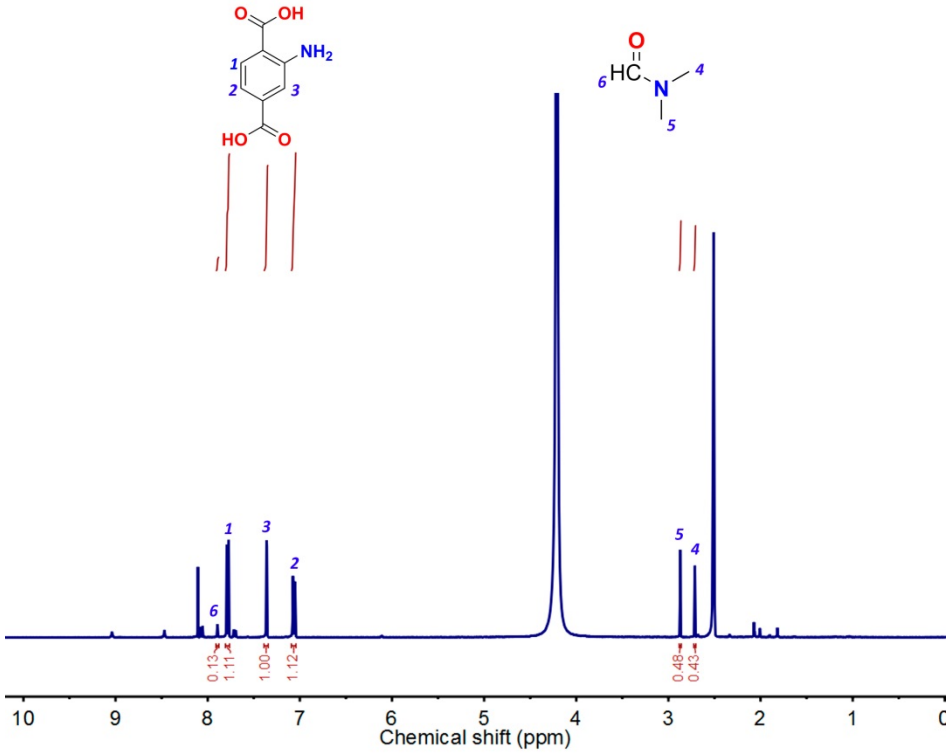

Section S5. ZIF-8/-67 characterization

Figure S25. (Top) Photographs of ZIF-8 powder before and after UV-Vis irradiation (500 mW·cm^{-2} for 30 min). (Bottom) Infrared camera images of ZIF-8 before and during UV-Vis irradiation.

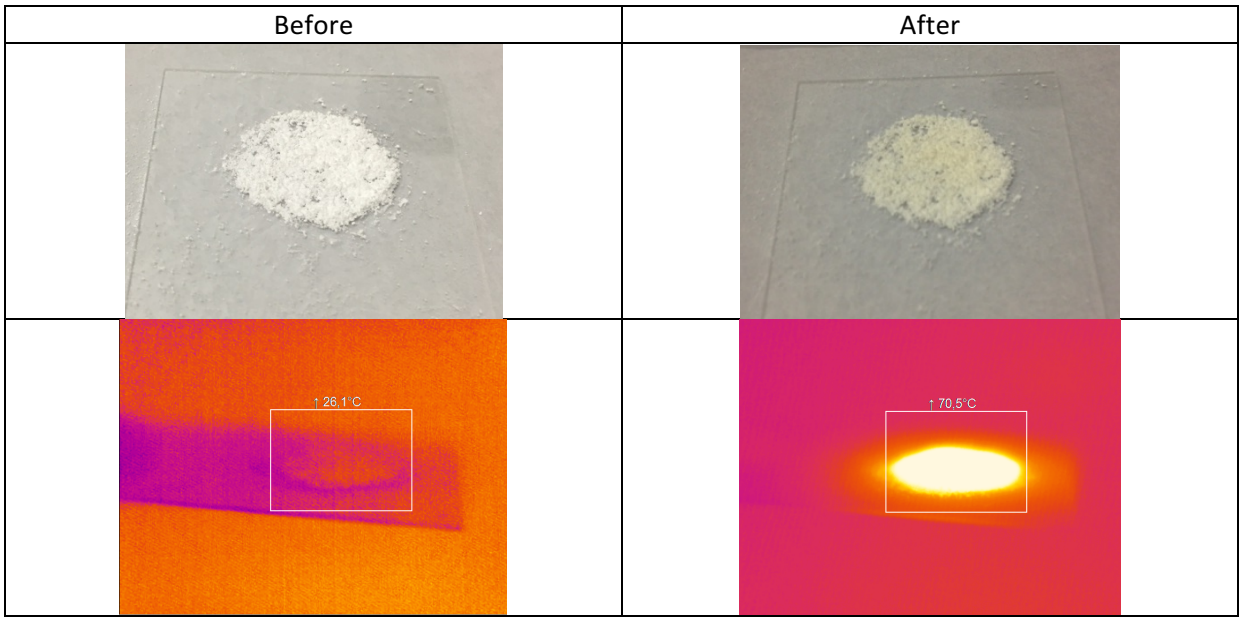

Figure S26. (Top) Photographs of ZIF-67 powder before and after UV-Vis irradiation (500 mW·cm^{-2} for 30 min). (Bottom) Infrared camera images of ZIF-67 before and during UV-Vis irradiation.

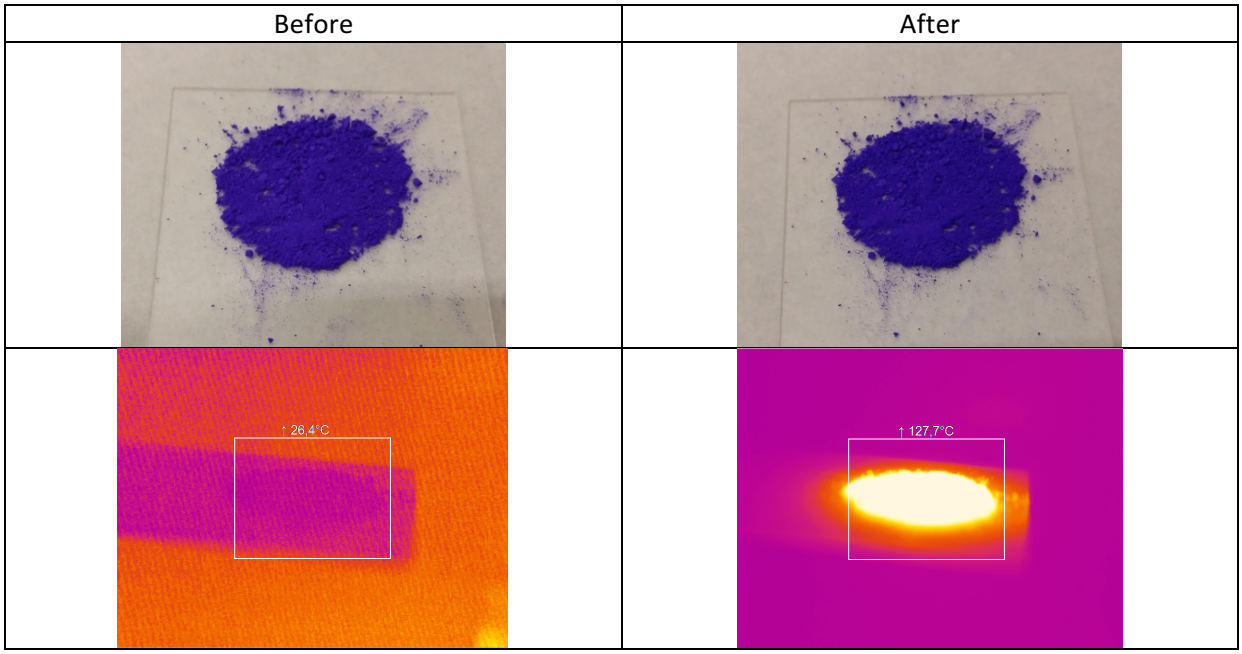

Figure S27. Solid-state UV-Vis spectra of ZIF-8 (red) and 2-methylimidazole (2-MIM) (black).

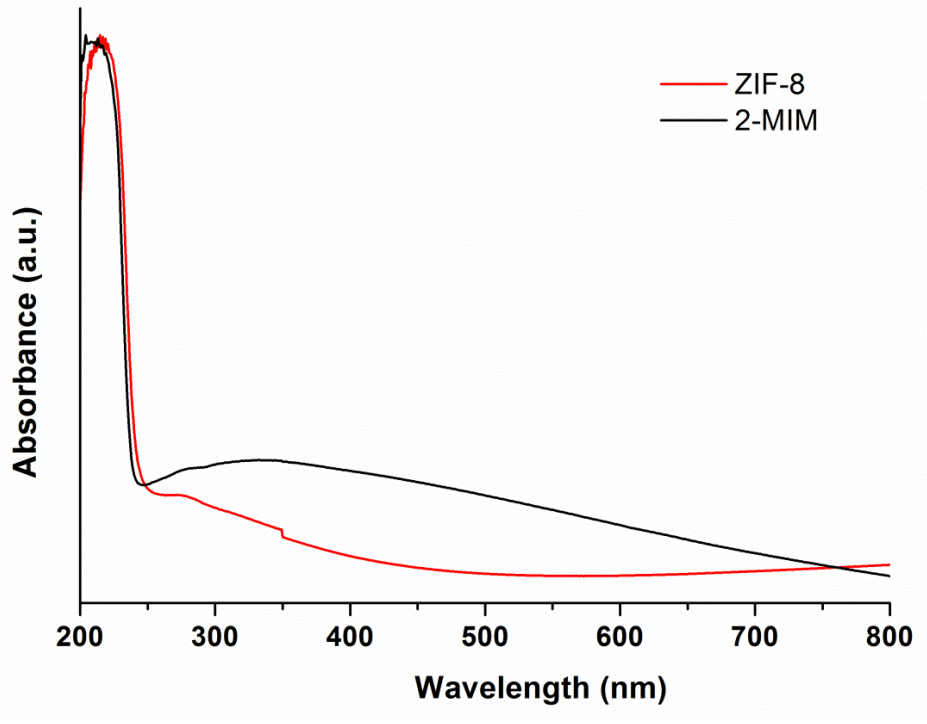

Figure S28. Solid-state UV-Vis spectra of ZIF-67 (red) and 2-methylimidazole (2-MIM) (black).

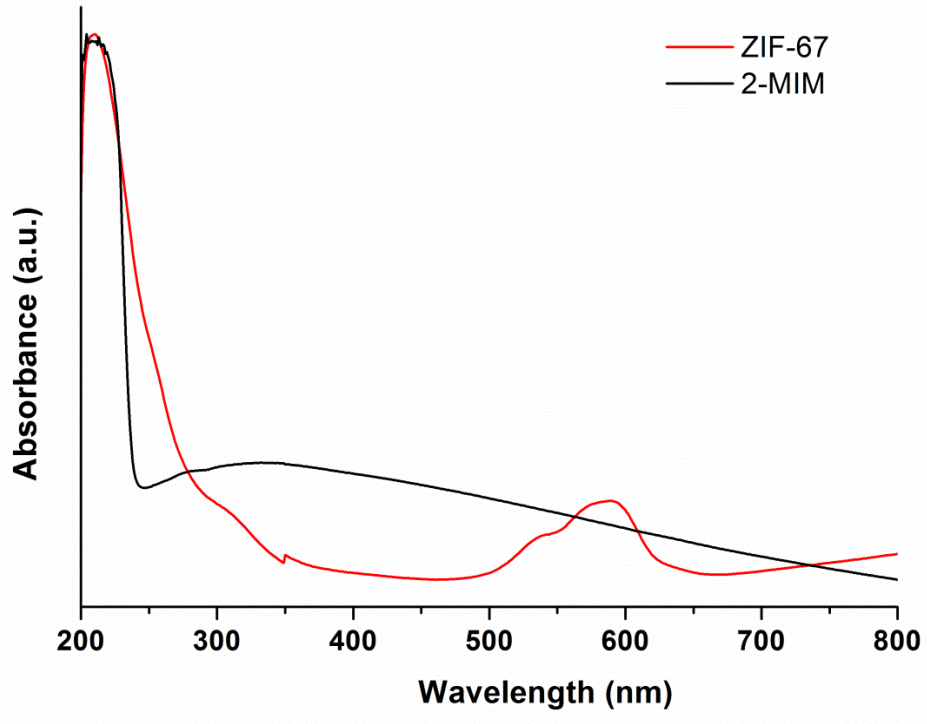

Figure S29. XRPD patterns of ZIF-8 simulated (black), as made (red) and after UV-Vis irradiation at 500 mW·cm^{-2} for 30 min (blue).

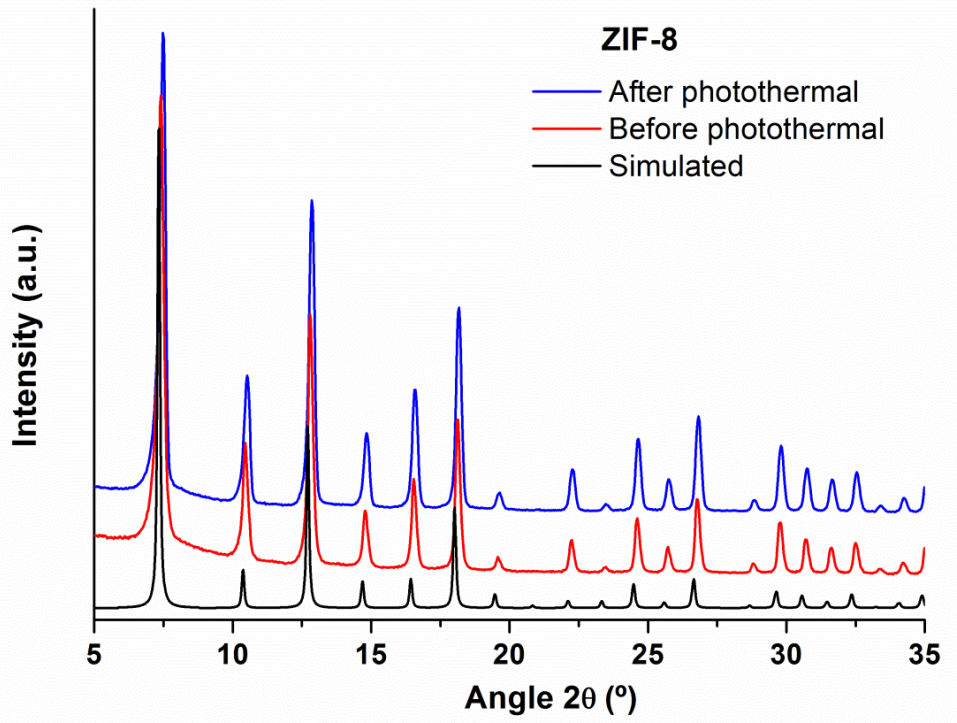

Figure S30. XRPD patterns of ZIF-67 simulated (black), as made (red) and after UV-Vis irradiation at 500 mW·cm^{-2} for 30 min (blue).

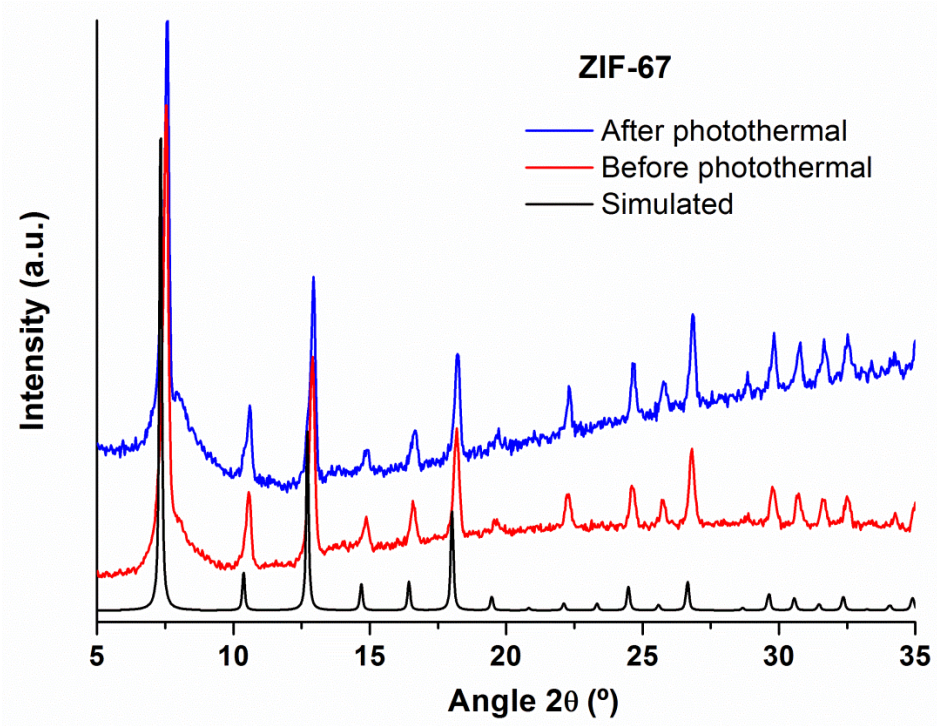

Figure S31. N_2 adsorption isotherm and linear fit of the pressure range used to calculate BET area for ZIF-8 after UV-Vis irradiation at 500 mW·cm^{-2} for 30 min.

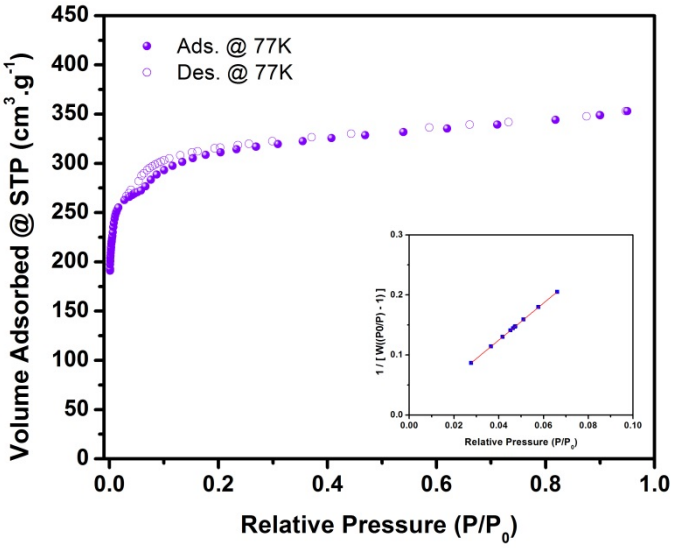

BET surface area: 1129.981 m²·g^{-1}

Slope: 3.080 g·cm^{-3} STP

Intercept: 1.548e-03 g·cm^{-3} STP

Correlation coefficient: 0.999970

C constant: 1991.243

Molecular cross-sectional area: 0.1620 nm²

Figure S32. N_2 adsorption isotherm and linear fit of the pressure range used to calculate BET area for ZIF-67 after UV-Vis irradiation at 500 mW·cm^{-2} for 30 min.

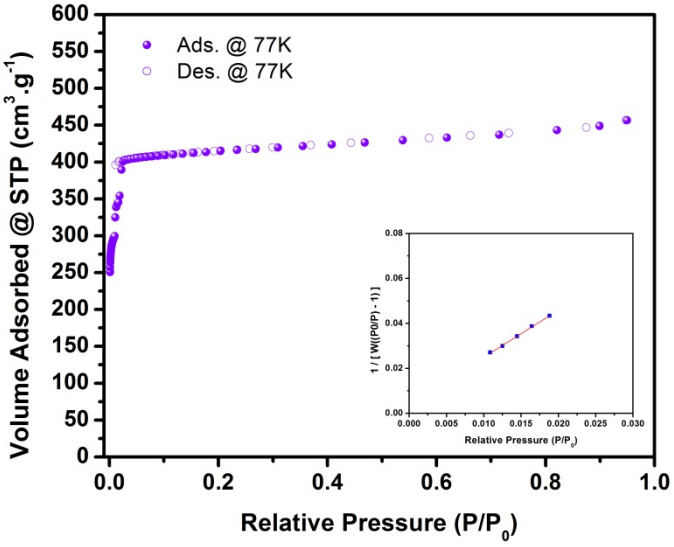

BET surface area: 1665.865 m²·g^{-1}

Slope: 2.086 g·cm^{-3} STP

Intercept: 4.137e-03 g·cm^{-3} STP

Correlation coefficient: 0.999273

C constant: 505.357

Molecular cross-sectional area: 0.1620 nm²

Figure S33. ^{1}H NMR spectrum of the photothermally activated ZIF-8 once digested in DCl/DMSO-d_6.

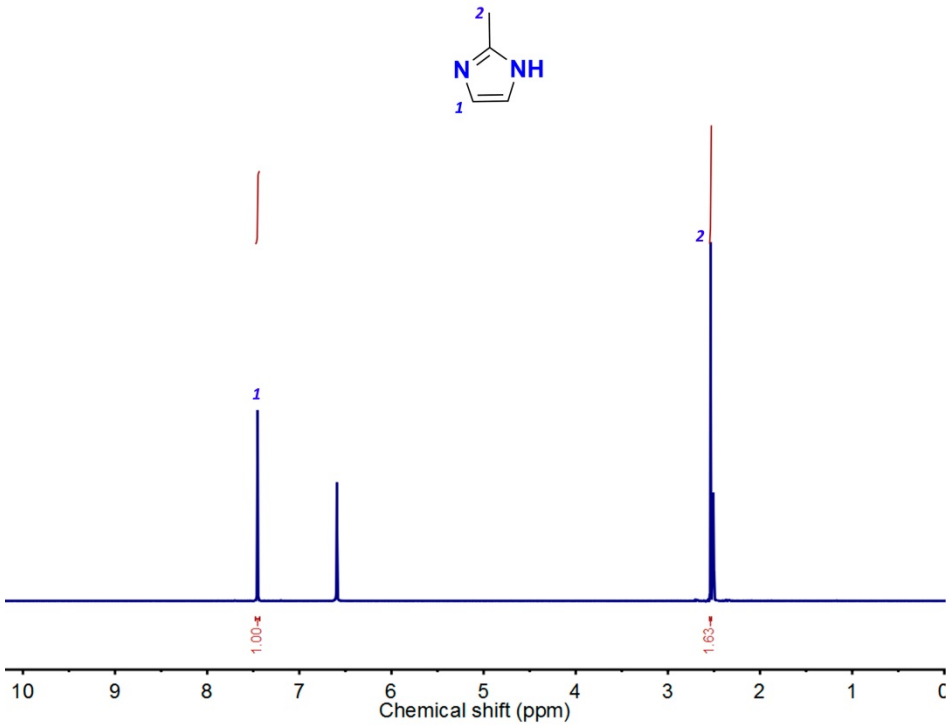

Figure S34. ^{1}H NMR spectrum of the photothermally activated ZIF-67 once digested in DCl/DMSO-d_6.

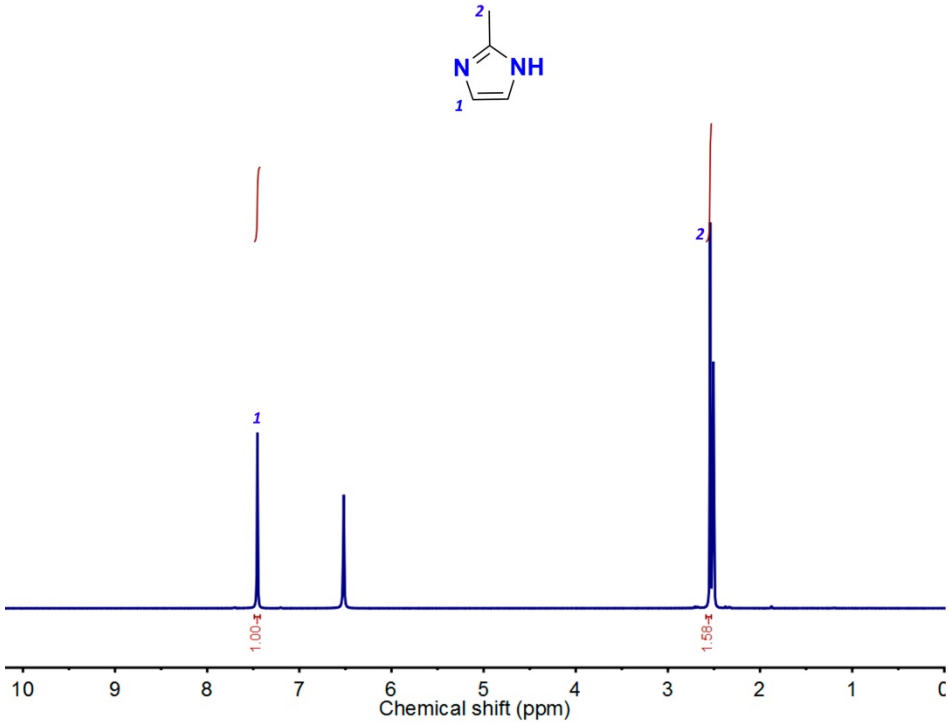

Section S6. Fe-MIL-NH_2 characterization

Figure S35. (Top) Photographs of Fe-MIL-NH_2 powder before and after UV-Vis irradiation (500 $mW \cdot cm^{-2}$ for 30 min). (Bottom) Infrared camera images of Fe-MIL-NH_2 before and during UV-Vis irradiation.

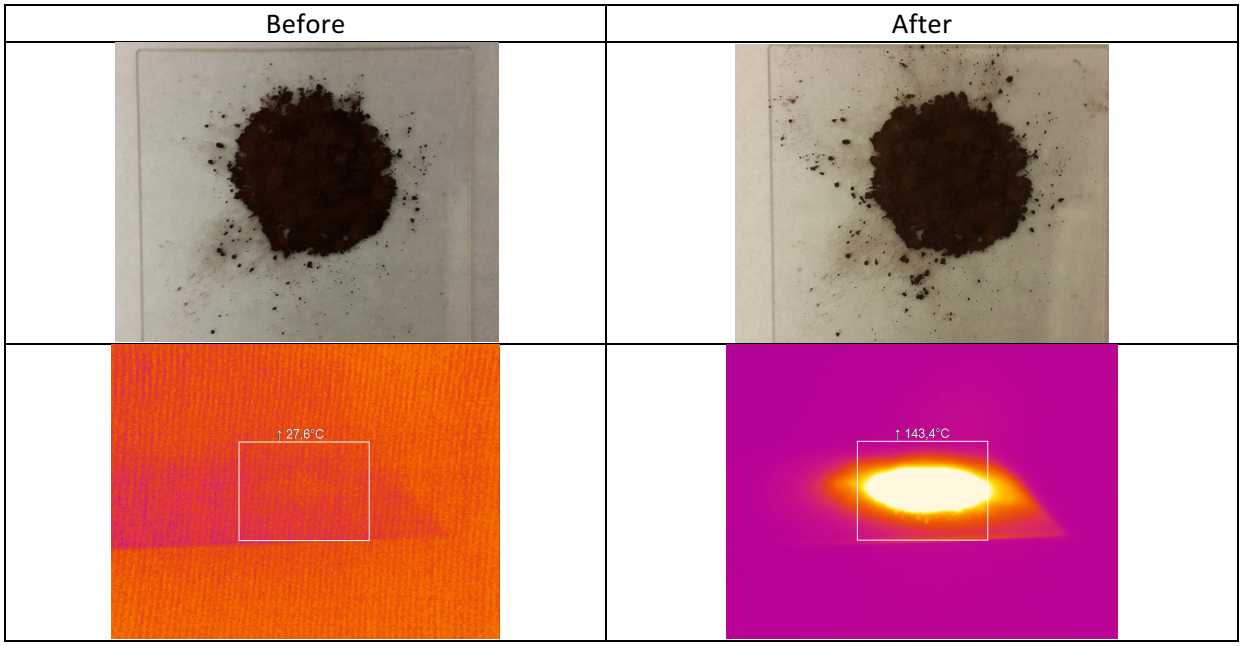

Figure S36. Solid-state UV-Vis spectra of Fe-MIL-NH_2 (red) and 2-aminoterephtalic acid (BDC-NH_2) (black).

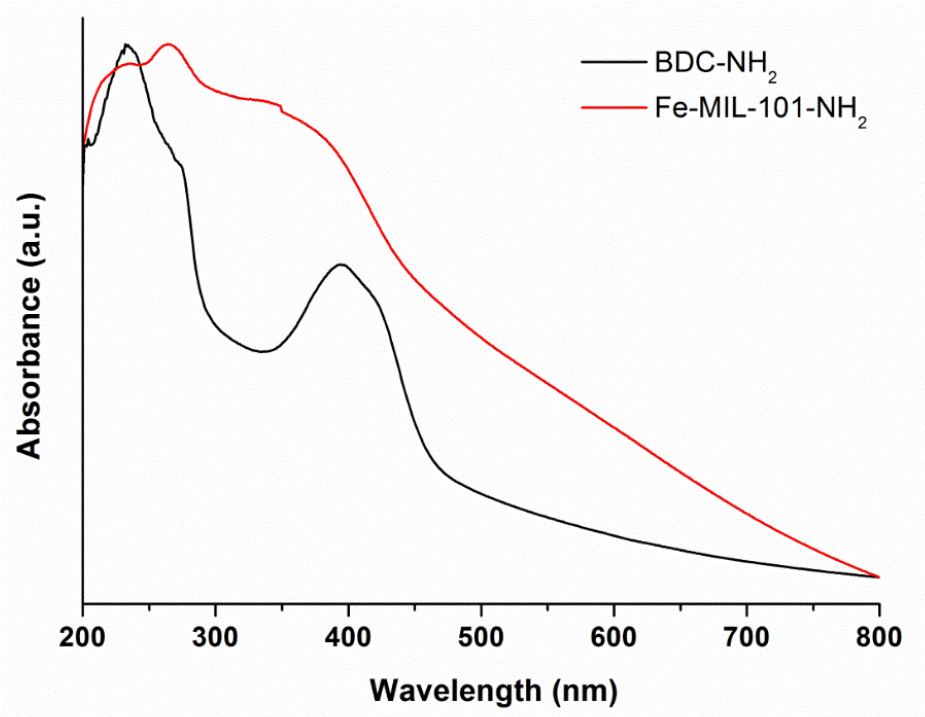

Figure S37. XRPD patterns of Fe-MIL-NH_2 simulated (black), as made (red) and after UV-Vis irradiation at 500 mW·cm^{-2} for 30 min (blue).

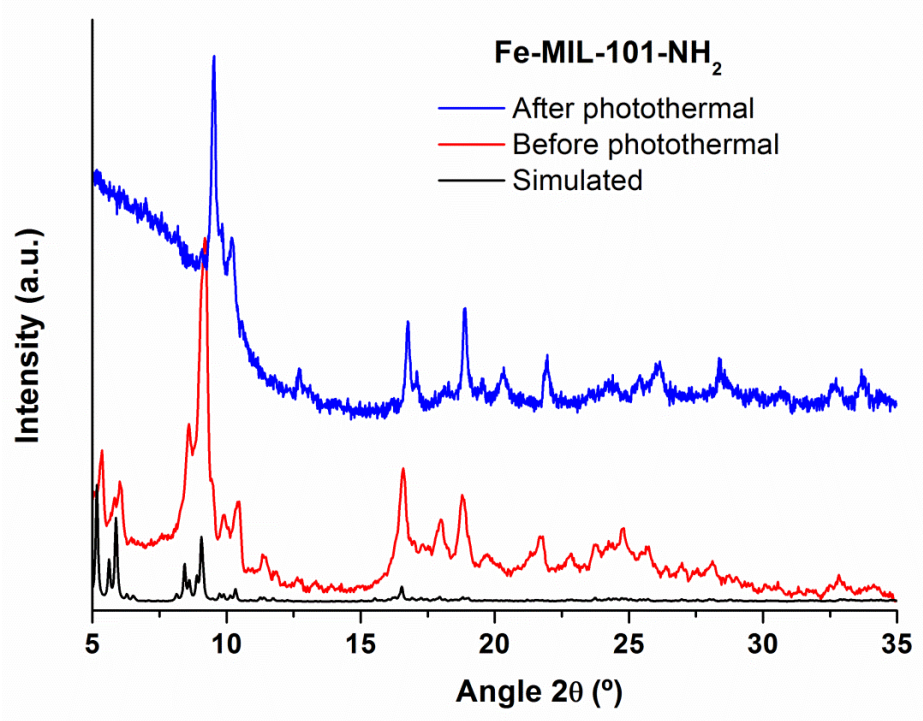

Figure S38. N_2 adsorption isotherm and linear fit of the pressure range used to calculate BET area for Fe-MIL-NH_2 after UV-Vis irradiation at 500 mW·cm^{-2} for 30 min.

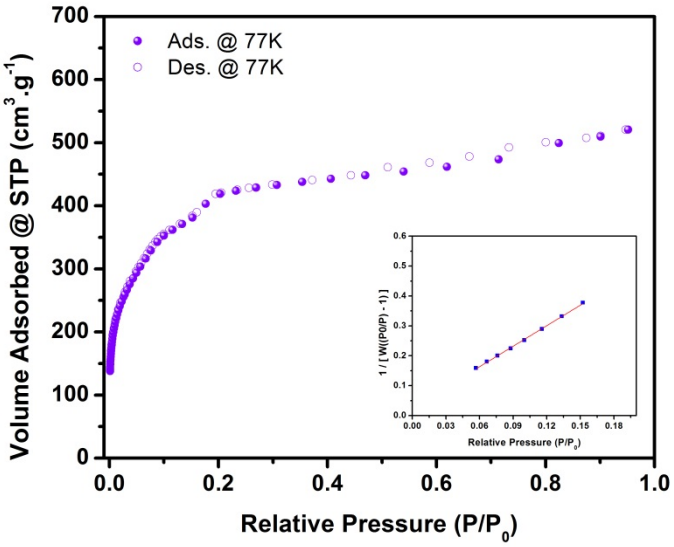

BET surface area: 1505.629 $m^2 \cdot g^{-1}$

Slope: 2.287 $g \cdot cm^{-3}$ STP

Intercept: 2.639e-02 $g \cdot cm^{-3}$ STP

Correlation coefficient: 0.999569

C constant: 87.662

Molecular cross-sectional area: 0.1620 nm^2

Figure S39. ^{1}H NMR spectrum of the photothermally activated Fe-MIL-NH_2 once digested in NaOD/D_2O.

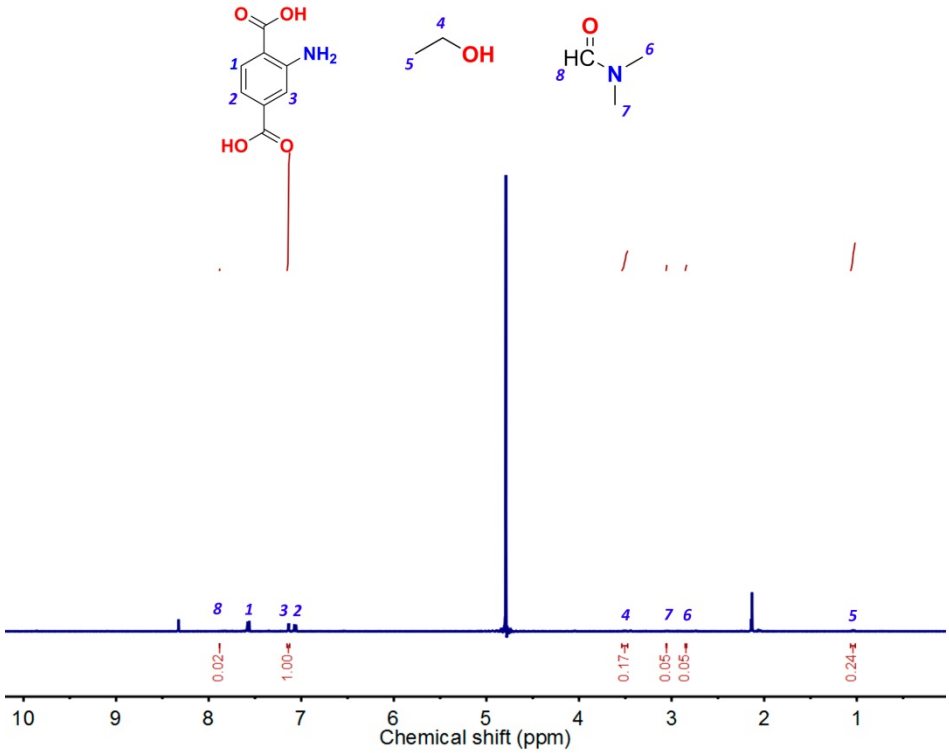

Section S7. IRMOF-3 characterization

Figure S40. (Top) Photographs of IRMOF-3 powder before and after UV-Vis irradiation (500 mW·cm^{-2} for 30 min). (Bottom) Infrared camera images of IRMOF-3 before and during UV-Vis irradiation.

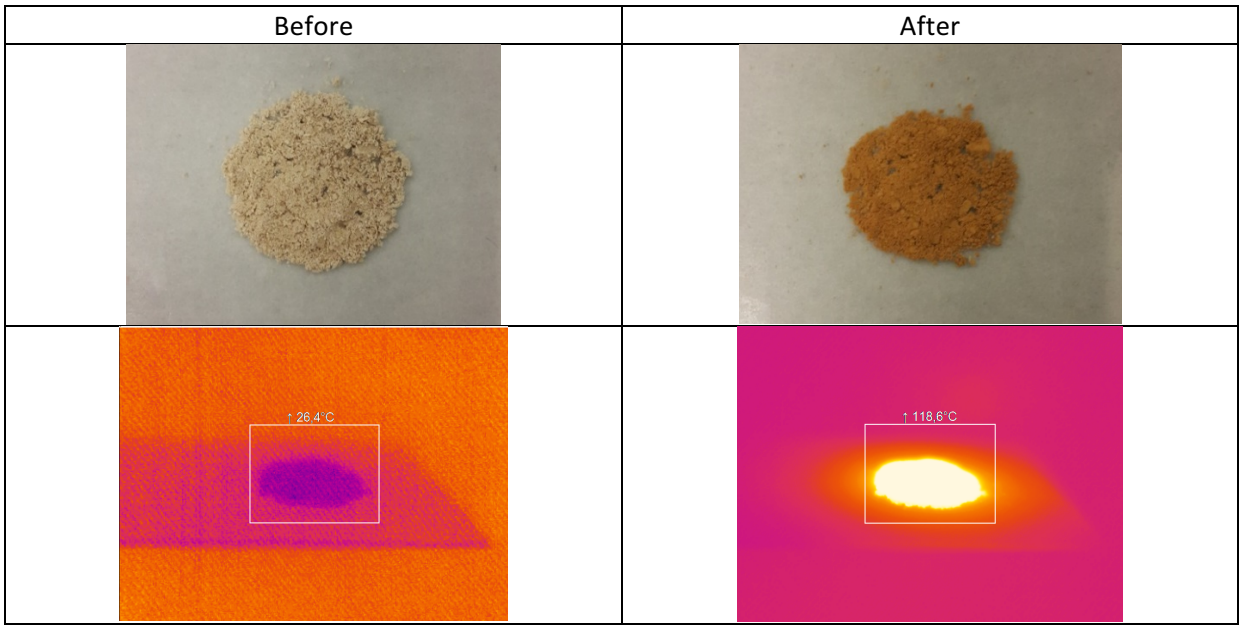

Figure S41. Solid-state UV-Vis spectra of IRMOF-3 (red) and 2-aminoterephtalic acid (BDC-NH_2) (black).

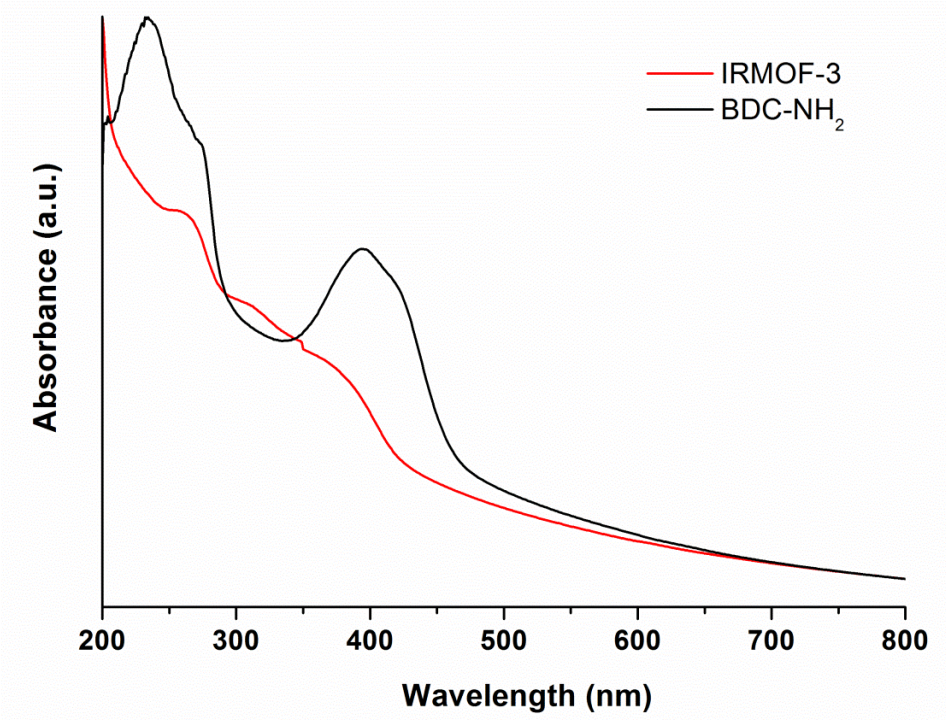

Figure S42. XRPD patterns of IRMOF-3 simulated (black), as made (red) and after UV-Vis irradiation at 500 mW·cm^{-2} for 30 min (blue).

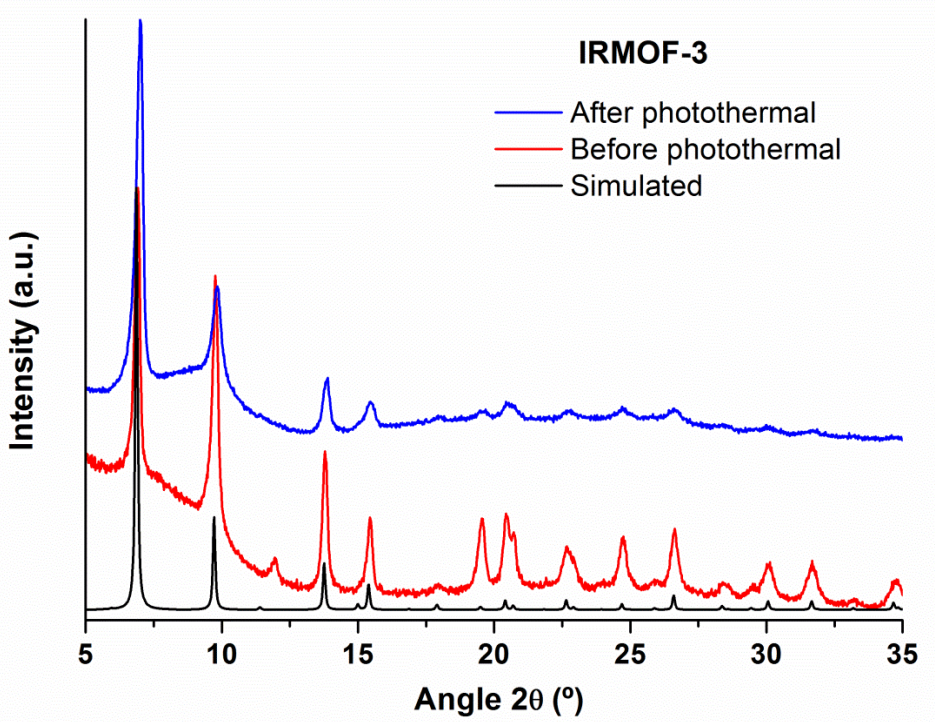

Figure S43. N_2 adsorption isotherm and linear fit of the pressure range used to calculate BET area for IRMOF-3 after UV-Vis irradiation at 500 mW·cm^{-2} for 30 min.

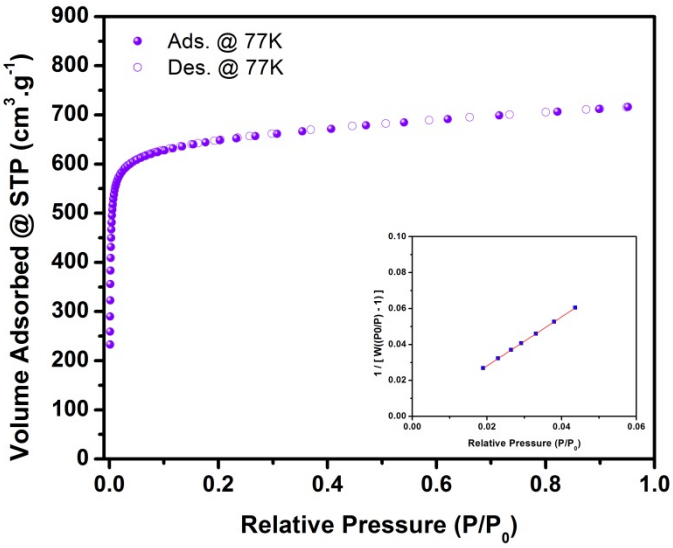

BET surface area: 2554.848 m²·g^{-1}

Slope: 1.362 g·cm^{-3} STP

Intercept: 9.037e-04 g·cm^{-3} STP

Correlation coefficient: 0.999995

C constant: 1508.365

Molecular cross-sectional area: 0.1620 nm²

Figure S44. ^{1}H NMR spectrum of the photothermally activated IRMOF-3 once digested in DCl/DMSO-d_6.

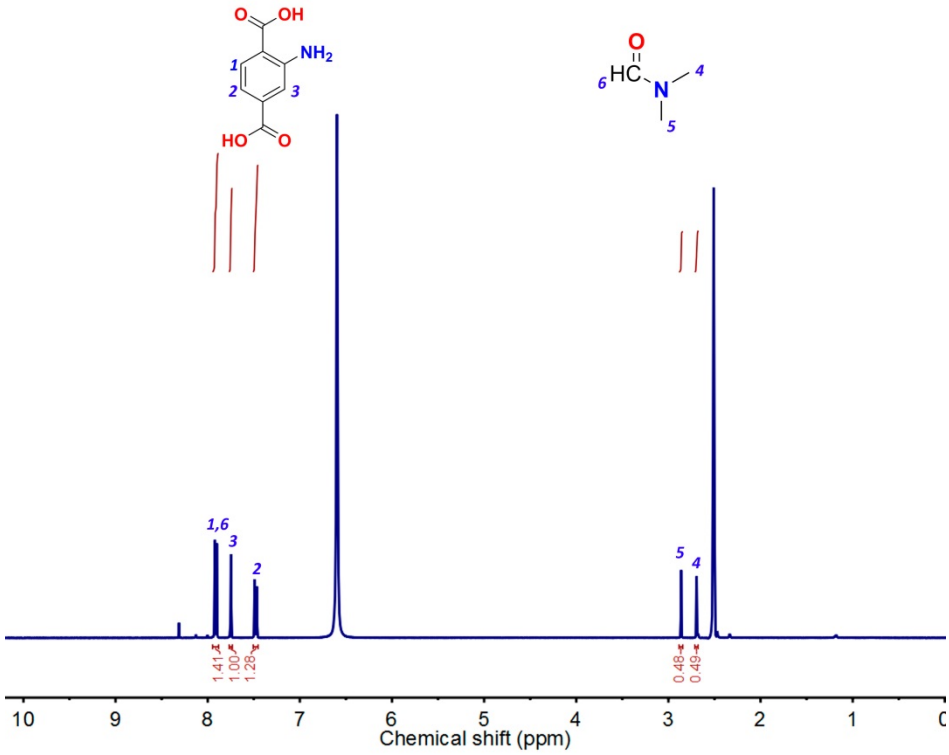

Section S8. CPO-27-M characterization

Figure S45. (Top) Photographs of CPO-27-Zn powder before and after UV-Vis irradiation (500 mW·cm^{-2} for 30 min). (Bottom) Infrared camera images of CPO-27-Zn before and during UV-Vis irradiation.

Before	After
	
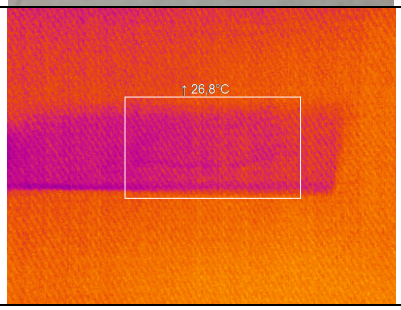	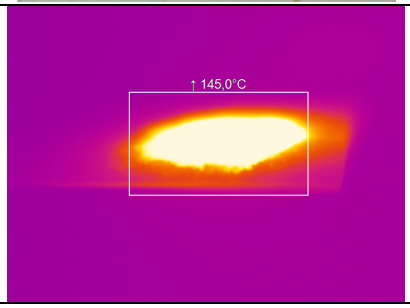

Figure S46. (Top) Photographs of CPO-27-Ni powder before and after UV-Vis irradiation (500 mW·cm^{-2} for 30 min). (Bottom) Infrared camera images of CPO-27-Ni before and during UV-Vis irradiation.

Before	After
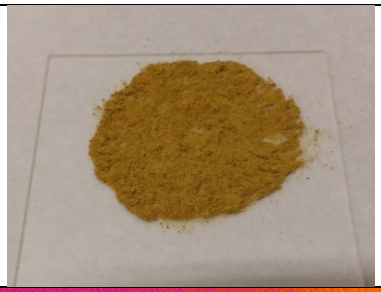	
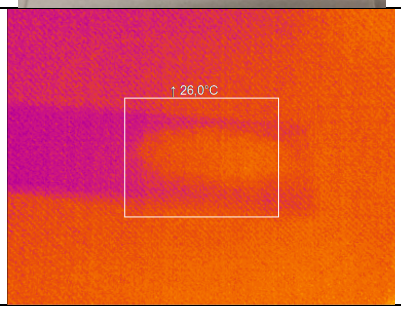	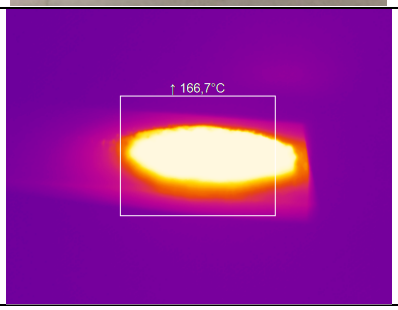

Figure S47. (Top) Photographs of CPO-27-Mg powder before and after UV-Vis irradiation (500 $mW \cdot cm^{-2}$ for 30 min). (Bottom) Infrared camera images of CPO-27-Mg before and during UV-Vis irradiation.

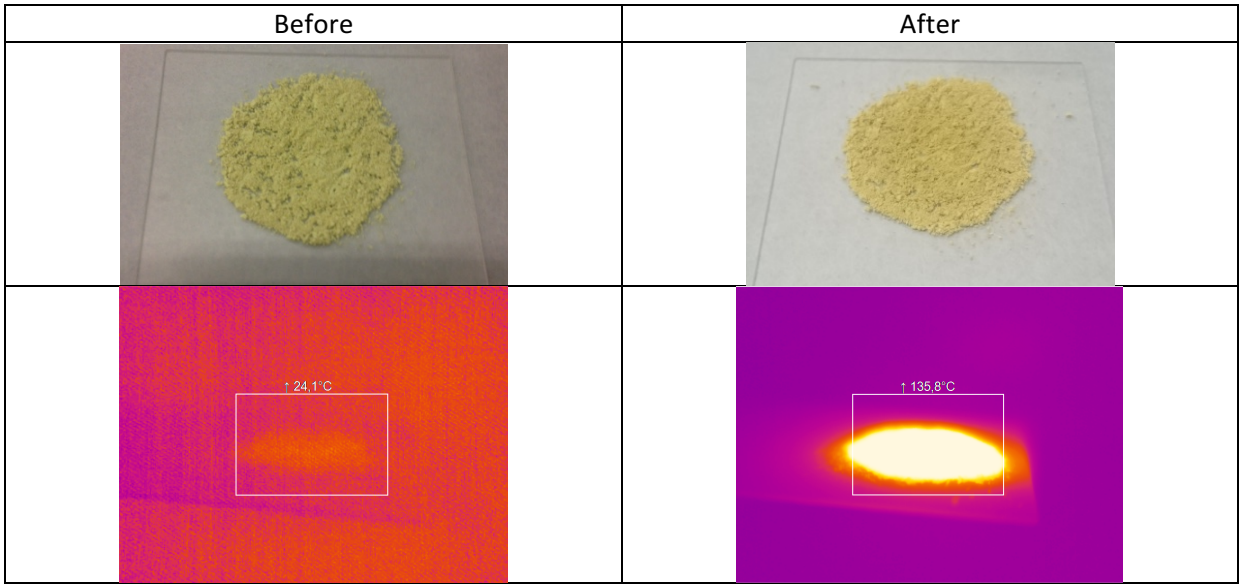

Figure S48. Solid-state UV-Vis spectra of CPO-27-Ni (red), CPO-27-Zn (blue), CPO-27-Mg (green) and 2,5-dihydroxyterephtalic acid (DHTA)(black).

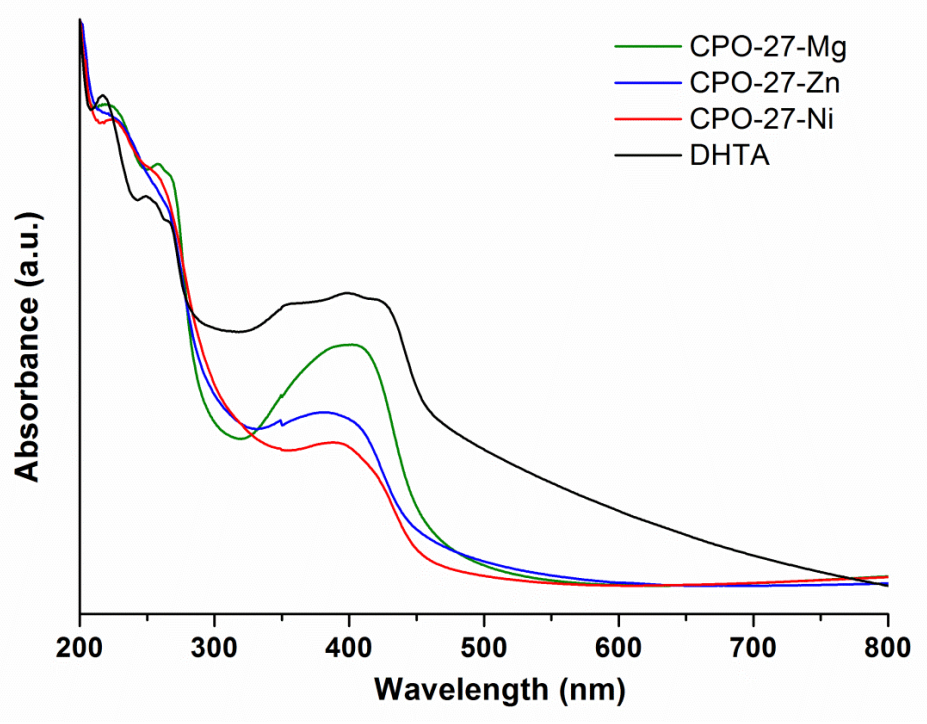

Figure S49. XRPD patterns of CPO-27-Zn simulated (black), as made (red) and after UV-Vis irradiation at 500 mW·cm^{-2} for 30 min (blue).

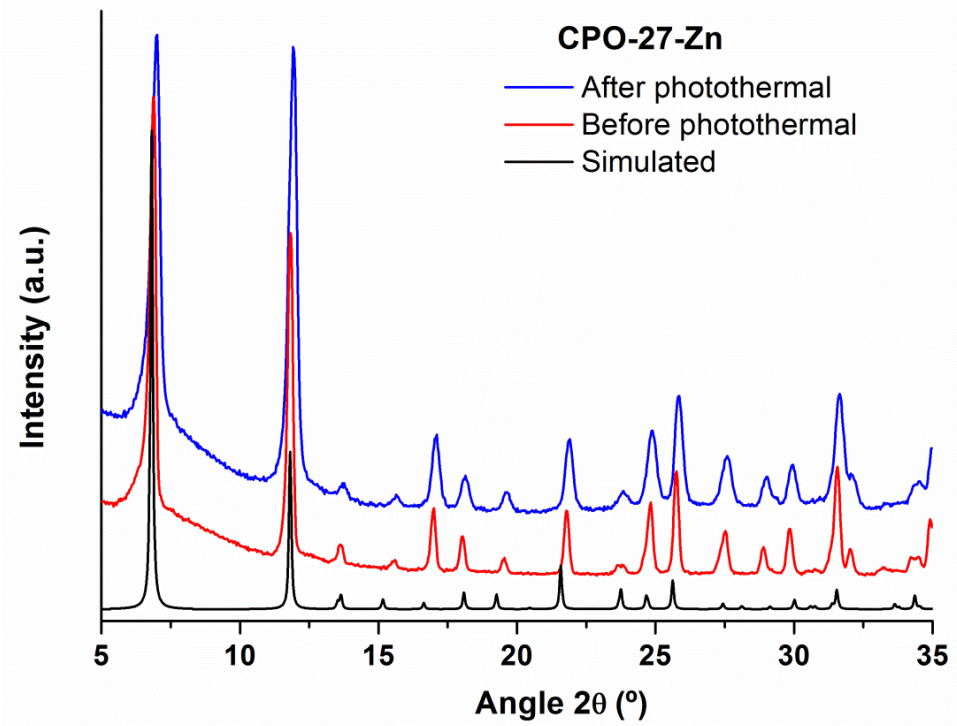

Figure S50. XRPD patterns of CPO-27-Ni simulated (black), as made (red) and after UV-Vis irradiation at 500 mW·cm^{-2} for 30 min (blue).

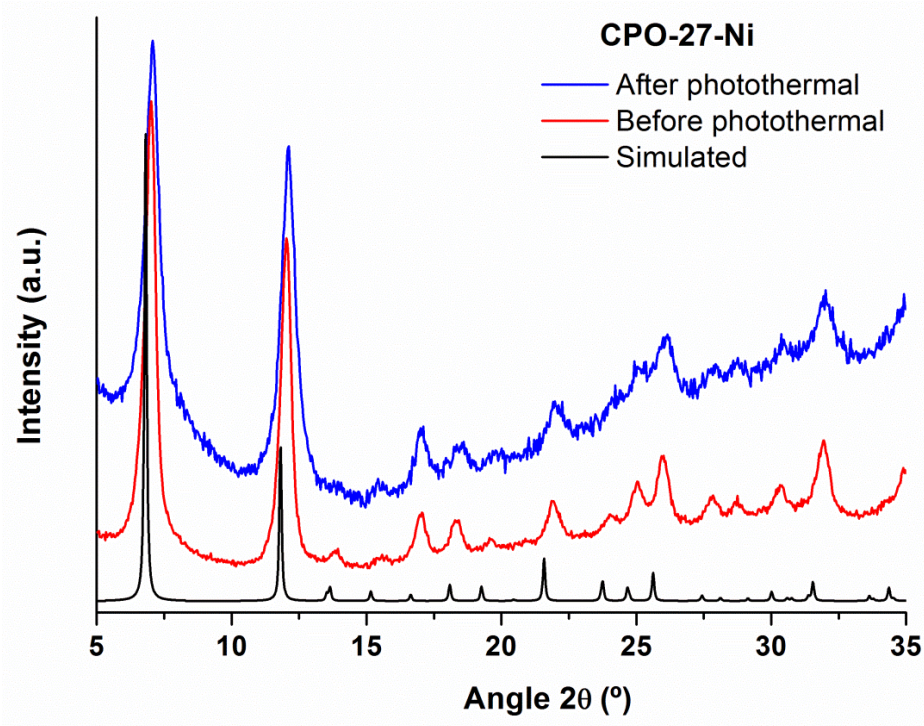

Figure S51. XRPD patterns of CPO-27-Mg simulated (black), as made (red) and after UV-Vis irradiation at 500 mW·cm^{-2} for 30 min (blue).

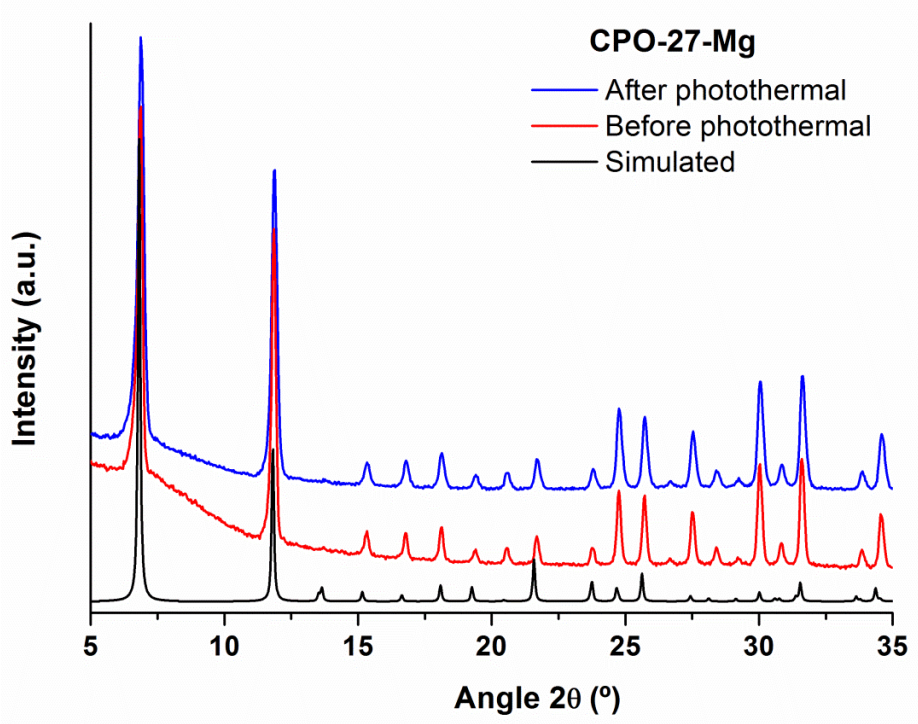

Figure S52. N_2 adsorption isotherm and linear fit of the pressure range used to calculate BET area for CPO-27-Zn after UV-Vis irradiation at 500 mW·cm^{-2} for 30 min.

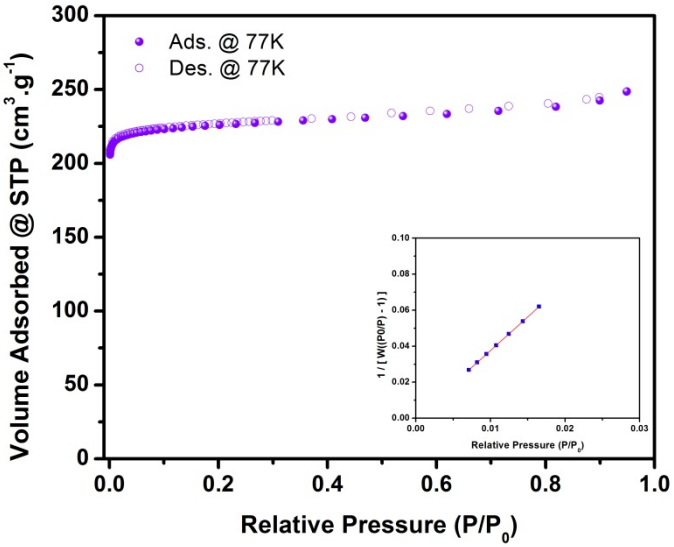

BET surface area: 931.767 m²·g^{-1}

Slope: 3.737 g·cm^{-3} STP

Intercept: 1.995e-04 g·cm^{-3} STP

Correlation coefficient: 0.999999

C constant: 18737.509

Molecular cross-sectional area: 0.1620 nm²

Figure S53. N_2 adsorption isotherm and linear fit of the pressure range used to calculate BET area for CPO-27-Ni after UV-Vis irradiation at 500 mW·cm^{-2} for 30 min.

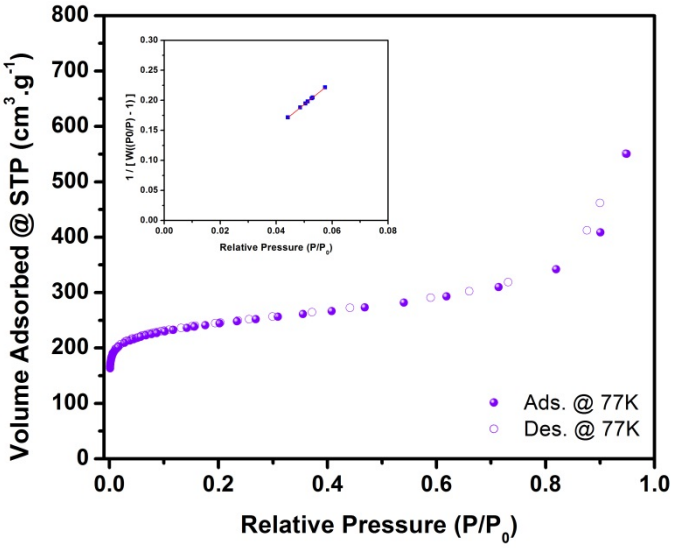

BET surface area: 922.311 m²·g^{-1}

Slope: 3.771 g·cm^{-3} STP

Intercept: 4.569e-03 g·cm^{-3} STP

Correlation coefficient: 0.999962

C constant: 826.387

Molecular cross-sectional area: 0.1620 nm²

Figure S54. N_2 adsorption isotherm and linear fit of the pressure range used to calculate BET area for CPO-27-Mg after UV-Vis irradiation at 500 mW·cm^{-2} for 30 min.

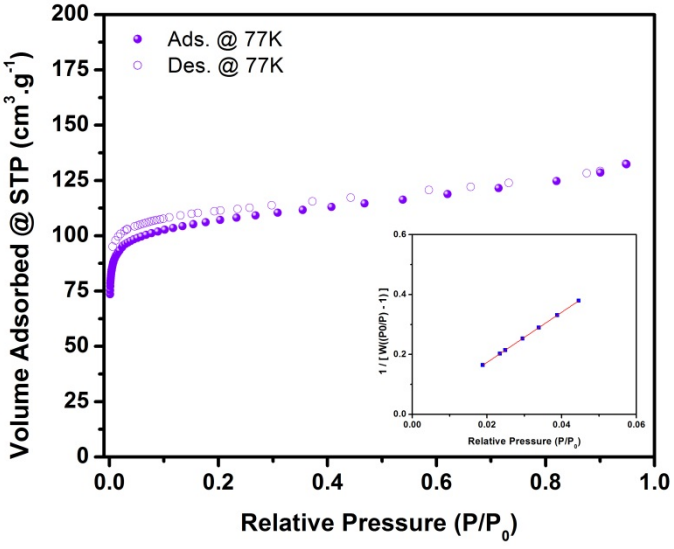

BET surface area: 415.707 m²·g^{-1}

Slope: 8.371 g·cm^{-3} STP

Intercept: 6.094e-03 g·cm^{-3} STP

Correlation coefficient: 0.999981

C constant: 1374.635

Molecular cross-sectional area: 0.1620 nm²

Figure S55. XRPD patterns of CPO-27-Mg simulated (black), and after UV-Vis irradiation at 500 mW·cm^{-2} (red), at 900 mW·cm^{-2} (blue) and at 2650 mW·cm^{-2} (green) for 30 min (blue).

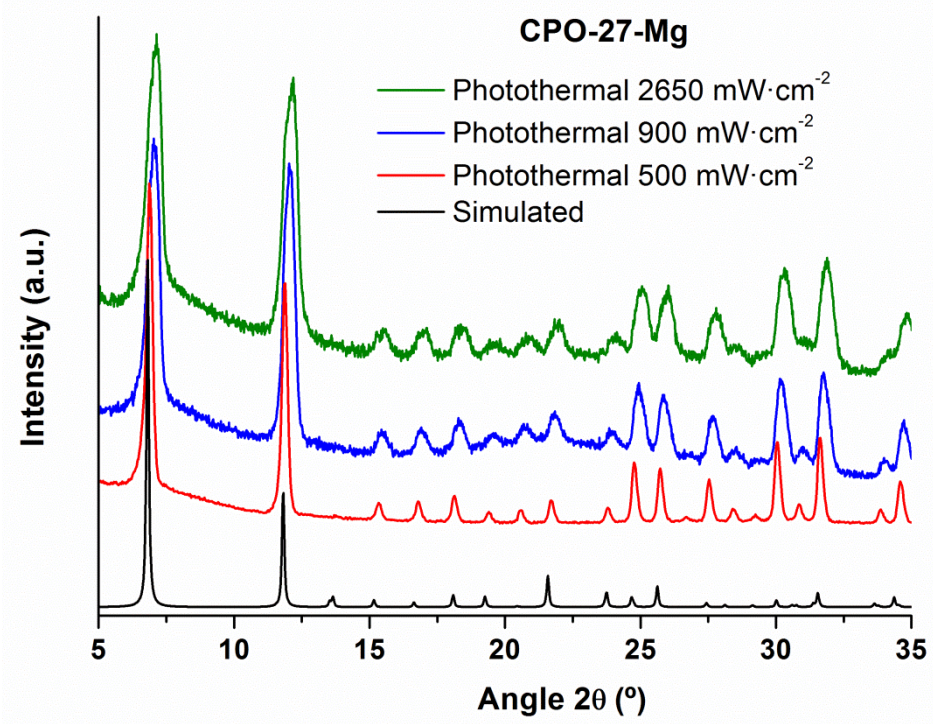

Figure S56. N_2 adsorption isotherm and linear fit of the pressure range used to calculate BET area for CPO-27-Mg after UV-Vis irradiation at 900 mW·cm^{-2} for 30 min.

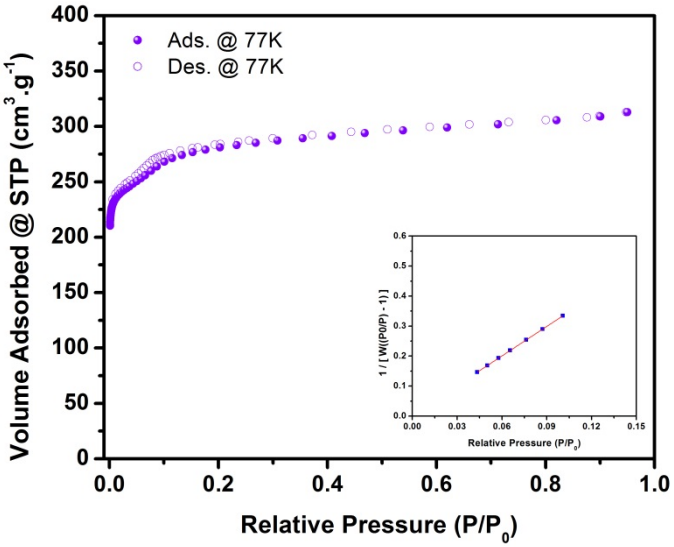

BET surface area: 1061.805 m²·g^{-1}

Slope: 3.275 g·cm^{-3} STP

Intercept: 4.312e-03 g·cm^{-3} STP

Correlation coefficient: 0.999995

C constant: 760.666

Molecular cross-sectional area: 0.1620 nm²

Figure S57. N_2 adsorption isotherm and linear fit of the pressure range used to calculate BET area for CPO-27-Mg after UV-Vis irradiation at 2650 mW·cm^{-2} for 30 min.

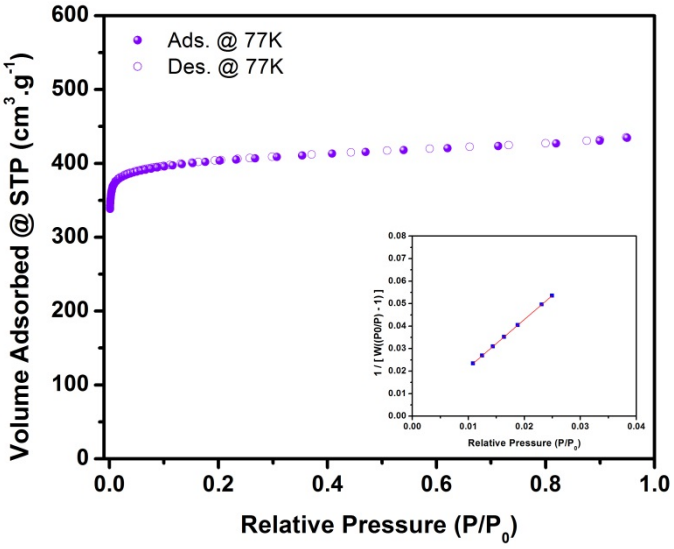

BET surface area: 1631.413 m²·g^{-1}

Slope: 2.134 g·cm^{-3} STP

Intercept: 2.517e-04 g·cm^{-3} STP

Correlation coefficient: 0.999999

C constant: 8481.353

Molecular cross-sectional area: 0.1620 nm²

Figure S58. ^{1}H NMR spectrum of the photothermally activated CPO-27-Zn once digested in DCl/DMSO-d$_6$.

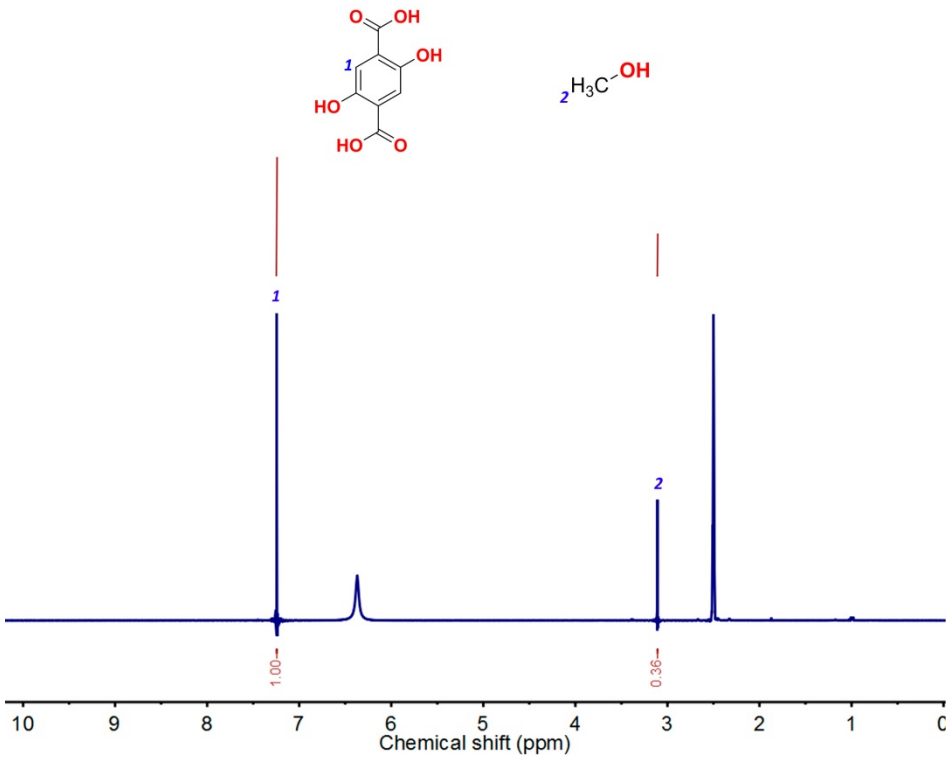

Figure S59. ^{1}H NMR spectrum of the photothermally activated CPO-27-Ni once digested in DCl/DMSO-d_6.

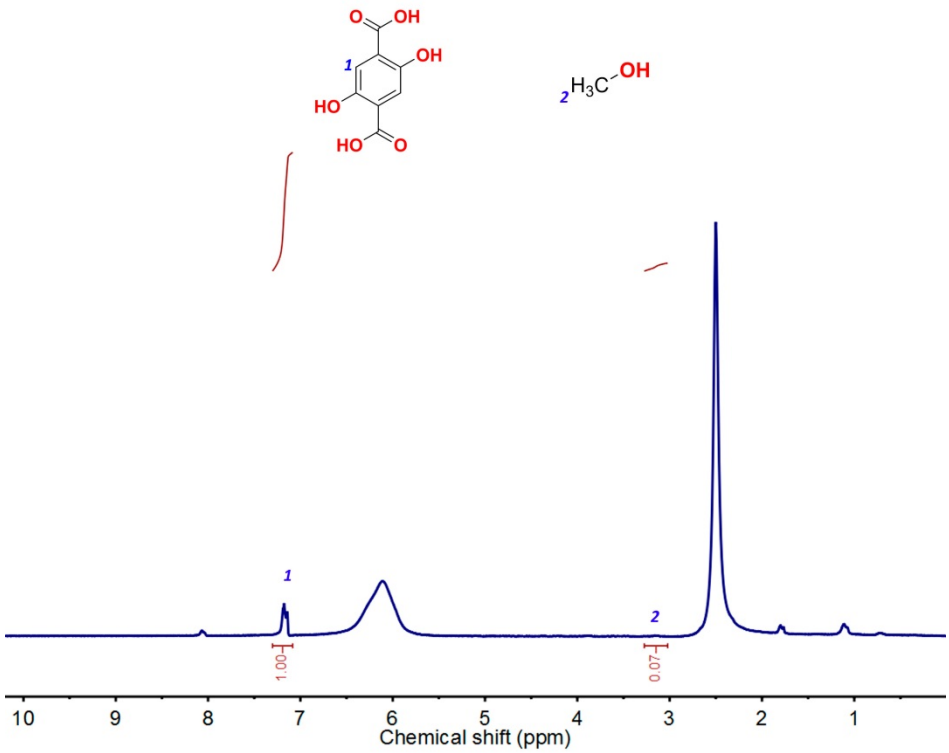

Figure S60. ^{1}H NMR spectrum of the photothermally activated CPO-27-Mg once digested in DCl/DMSO-d_6.

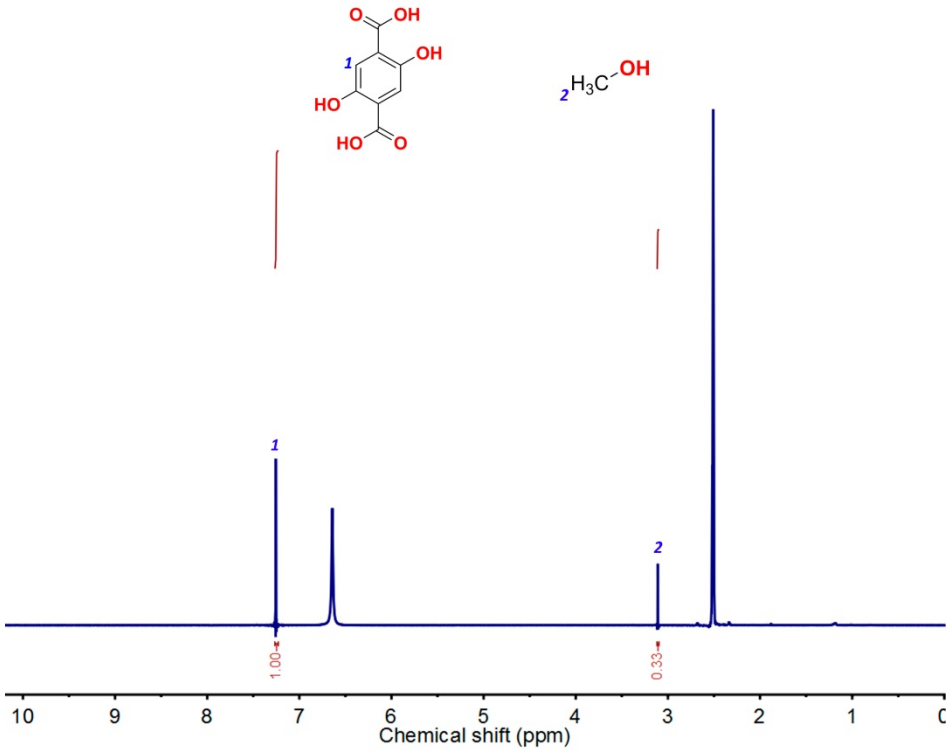

Section S9. COF-TAPB-BTCA characterization

Figure S61. Schematic representation of the synthesis of COF-TAPB-BTCA.

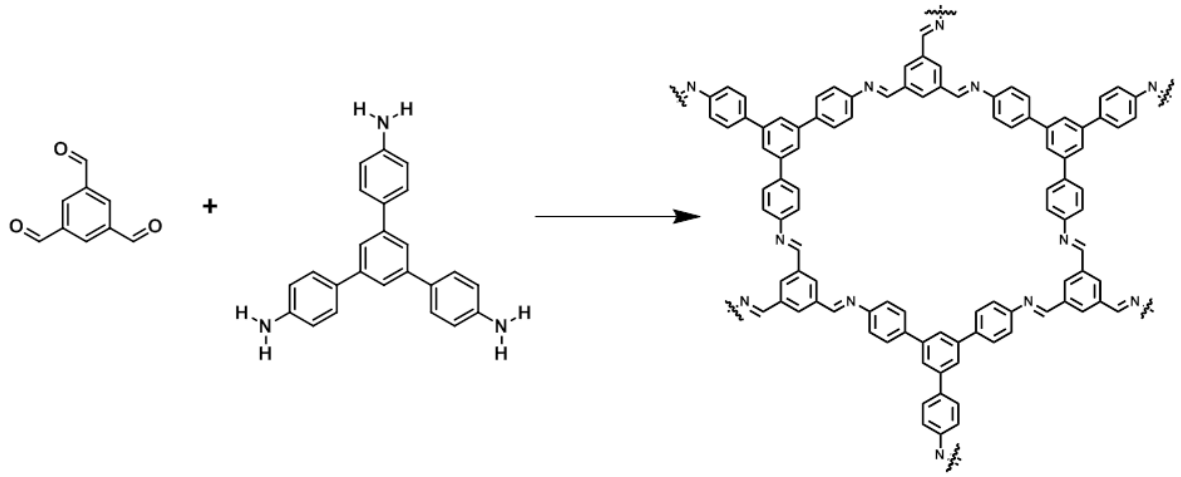

Figure S62. (Top) Photographs of COF-TAPB-BTCA powder before and after UV-Vis irradiation (500 mW·cm^{-2} for 30 min). (Bottom) Infrared camera images of COF-TAPB-BTCA before and during UV-Vis irradiation.

Before	After
	
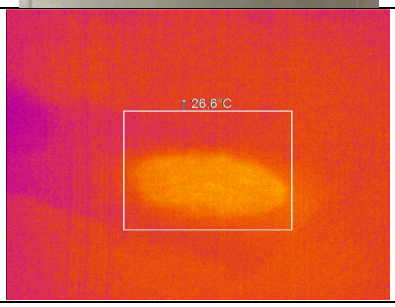	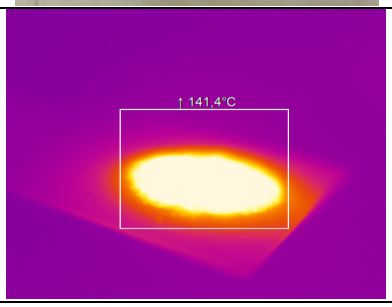

Figure S63. Solid-state UV-Vis spectra of COF-TAPB-BTCA (black), 1,3,5-benzenetricarbaldehyde (BTCA) (red) and 1,3,5,-tris-(4-aminophenyl)benzeneTAPB (blue).

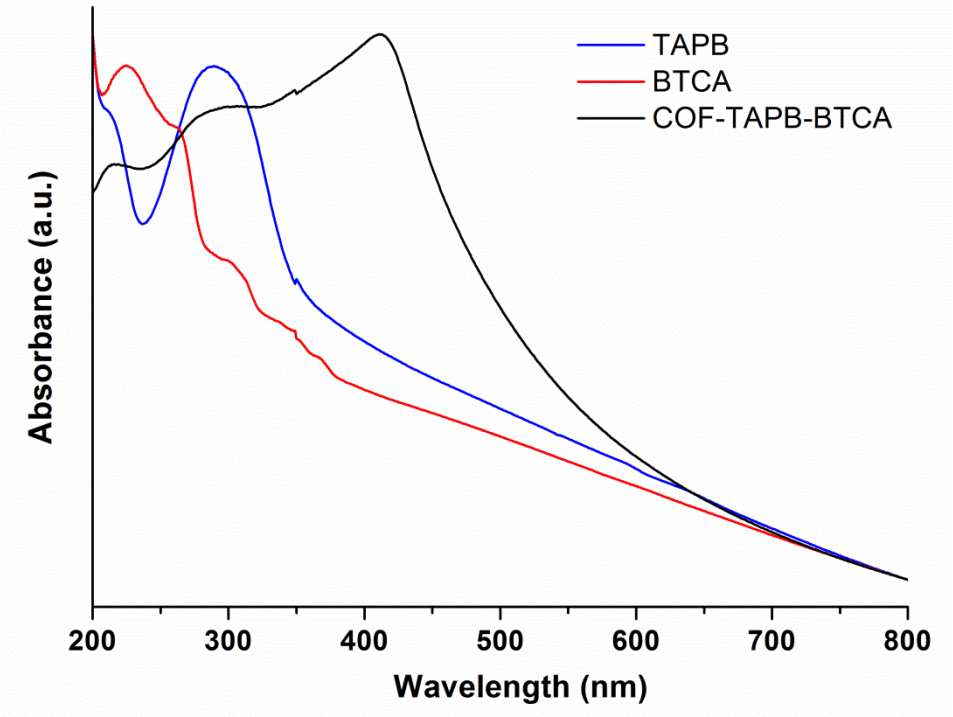

Figure S64. Temperature evolution as a function of time for COF-TAPB-BTCA irradiated at 500 $mW \cdot cm^{-2}$ for 30 min.

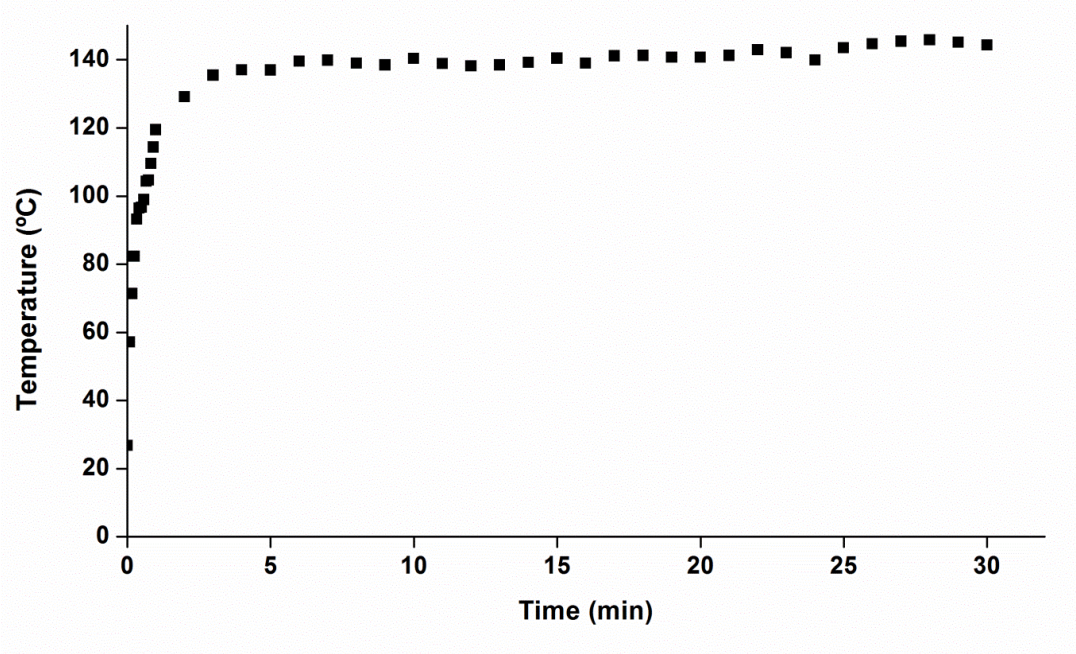

Figure S65. XRPD patterns of COF-TAPB-BTCA simulated (black), as made (red) and after UV-Vis irradiation at 500 mW·cm^{-2} for 30 min (blue).

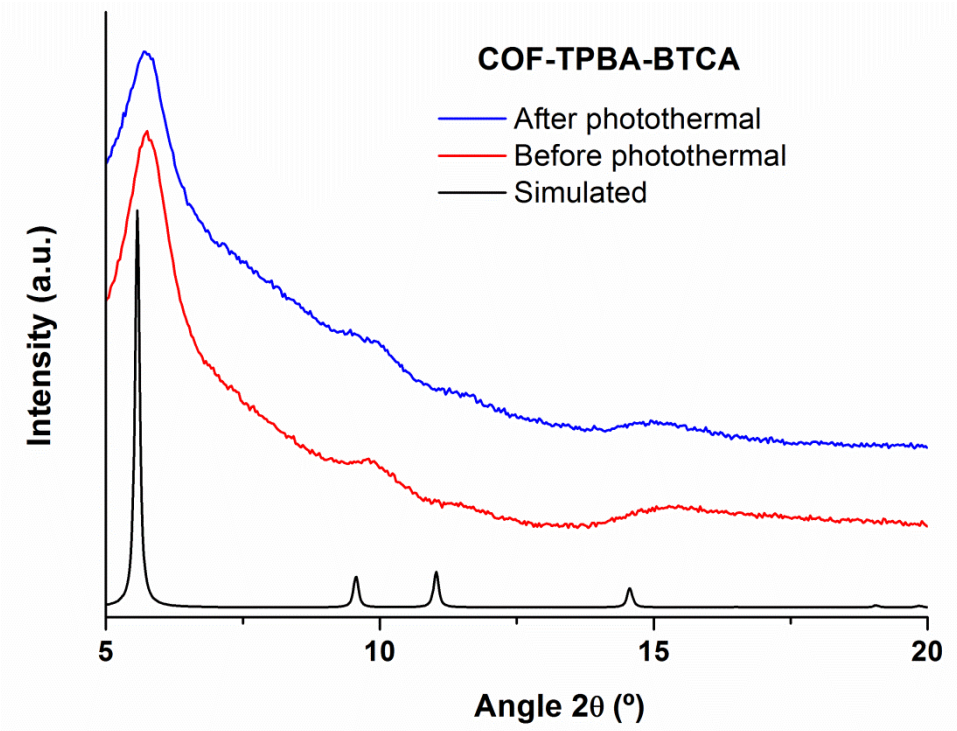

Figure S66. N_2 adsorption isotherm and linear fit of the pressure range used to calculate BET area for COF-TAPB-BTCA after UV-Vis irradiation at 500 mW·cm^{-2} for 30 min.

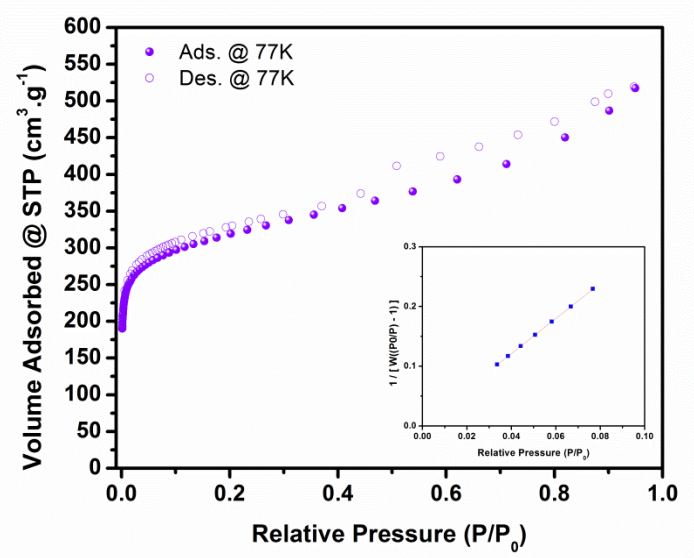

BET surface area: 1185.090 m²/g

Slope: 2.935 g/cm^3 STP

Intercept: 4.010e-03 g/cm^3 STP

Correlation coefficient: 0.999996

C constant: 732.811

Molecular cross-sectional area: 0.1620 nm²

Figure S67. ^{1}H NMR spectrum of the photothermally activated COF-TAPB-BTCA once digested in D_2SO_4/DMSO-d_6.

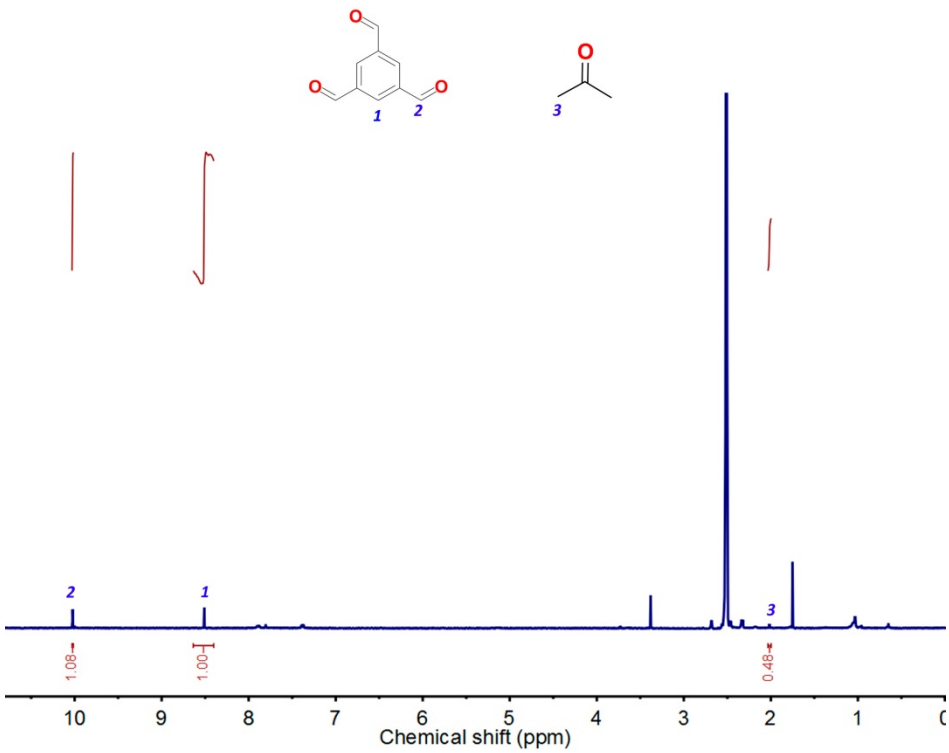

Section S10. Photothermal transduction efficiency (PTE) calculations

The PTE of all materials was calculated following the reported procedures in the literature.[1,2]

The system energy balance consists on:

$$\sum_i m_i C_{p,i} \frac{dT}{dt} = Q_{in,MOF} + Q_{in,surr} - Q_{out} \quad (1)$$

, where m_i and $C_{p,i}$ are the mass and heat capacity of the system components.

$Q_{in,MOF}$ is the heat input from the MOFs due to the photothermal effect according to Equation (2):

$$Q_{in,MOF} = I(1 - 10^{-A_\lambda})\eta \quad (2)$$

, where I is the light power, A_λ is the absorbance of the material at a certain wavelength, and η is the photothermal transduction efficiency. The light power was measured using the power-meter. At a distance of 7 cm, the light power was 500 mW. The term 10^{-A_λ} tends to 0 due to the high A_λ value of 100 mg used in our experimental setup.

$Q_{in,surr}$ is the heat input from the photothermal effect of the surroundings. In our case, there is only air between the light guide and the sample, which is not heated by the light source, thus not affecting the energy balance.

Q_{out} is the heat loss of the material to the surroundings, as defined by Equation (3):

$$Q_{out} = hA(T - T_{surr}) \quad (3)$$

, where T_{surr} is the room temperature, *h* is the heat-transfer coefficient, and *A* is the surface of the irradiated powder.

At the maximum temperature (T_{max}), the heat flux reaches a steady state, which allows balancing the energy input with energy output:

$$Q_{in,MOF} = Q_{out} \quad (4)$$

Substituting Equation 2 and 3 into Equation 4, Equation 5 is obtained:

$$\eta = \frac{hA(T_{max} - T_{surr})}{I} \quad (5)$$

The temperature increase as a function of time during light irradiation follows the expression:[1]

$$\frac{T_{amb} - T}{T_{amb} - T_{max}} = 1 - e^{(-t/\tau_s)} \quad (6)$$

, where τ_s is a time constant:

$$\tau_s = \frac{\sum_i m_i C_{p,i}}{hA} \quad (7)$$

Fitting the data (Equation (8)) of each material to a linear trend, we calculated τ_s:

$$\ln\left(1-\frac{T_{amb}-T}{T_{amb}-T_{max}}\right)=-t/\tau_s \quad (8)$$

Then, the heat transfer coefficient of each material was calculated using Equation (9):

$$hA=\frac{\sum_i m_i C_{p,i}}{\tau_s} \quad (9)$$

Finally, we substituted these values in Equation (10) to calculate each photothermal transduction efficiency:

$$\eta=\frac{hA(T_{max}-T_{surr})}{I} \quad (10)$$

Table S1. Summary of the obtained values for the PTE calculation.

Material	τ_s (sec)	Cp*	hA (mW/K)	T_{max}-T_{surr}	η (%)
HKUST-1	71.8	1.225	1.7	98.5	33.6
UiO-66	123.6	1.750	1.4	17.8	5.0
UiO-66-NH_2	60.9	1.607	2.6	112.5	59.3
ZIF-8	123.8	0.124	0.1	12.8	0.3
ZIF-67	43.4	1.084	2.5	100.1	50.0
IRMOF-3	71.0	1.062	1.5	86.1	25.8
MIL-101-NH_2	41.3	1.578	3.8	113.2	86.6
Zn-CPO-27	69.8	0.766	1.1	108.2	23.8
Ni-CPO-27	49.9	1.670	3.4	139.7	93.6
Mg-CPO-27	97.7	1.050	1.1	100.5	21.6
COF-TAPB-BTCA	47.2	1.185	2.5	110.4	55.4

* Cp values were determined from Differential Scanning Calorimetry (DSC) analysis.

References

1. Roper, D. K.; Ahn, W.; Hoepfner, M. Microscale Heat Transfer Transduced by Surface Plasmon Resonant Gold Nanoparticles. *J. Phys. Chem. C,* 2007, **111**, 3636-3641.
2. Wang, F.; Huang, Y.; Chai, Z.; Zeng, M.; Li, Q.; Wang, Y.; Xu, D. Photothermal-Enhanced Catalysis in Core-Shell Plasmonic Hierarchical Cu7S4 Microsphere@Zeolitic Imidazole Framework-8. *Chem. Sci.*, 2016, **7**, 6887.